Dissemination in time and space in presymptomatic *granulin* mutation carriers: a GENFI spatial chronnectome study

Enrico Premi,[1] Marcello Giunta,[2] Armin Iraji,[3] Srinivas Rachakonda,[3] Vince D. Calhoun,[3,4,5] Stefano Gazzina,[6] Alberto Benussi,[2] Roberto Gasparotti,[7] Silvana Archetti,[8] Martina Bocchetta,[9] Dave Cash, [9] Emily Todd, [9] Georgia Peakman, [9] Rhian Convery, [9] John C. van Swieten,[10] Lize Jiskoot,[10] Raquel Sanchez-Valle,[11] Fermin Moreno,[12] Robert Laforce,[13] Caroline Graff,[14] Matthis Synofzik,[15] Daniela Galimberti,[16,17] James B. Rowe,[18] Mario Masellis,[19] Carmela Tartaglia,[20] Elizabeth Finger,[21] Rik Vandenberghe,[22,23,24] Alexandre de Mendonça,[25] Fabrizio Tagliavini,[26] Chris R. Butler,[27] Isabel Santana,[28] Alexander Gerhard,[29] Isabelle Le Ber,[30,31,32,33] Florence Pasquier, Simon Ducharme,[34] Johannes Levin,[35] Adrian Danek,[36] Sandro Sorbi,[37,38] Markus Otto,[36] Jonathan D. Rohrer,[9] Barbara Borroni[2] on behalf of the Genetic Frontotemporal dementia Initiative (GENFI)^

1. Stroke Unit, Azienda Socio Sanitaria Territoriale Spedali Civili Brescia, Brescia, Italy;
2. Centre for Neurodegenerative Disorders, Department of Clinical and Experimental Sciences, University of Brescia, Brescia, Italy;
3. Tri-institutional Center for Translational Research in Neuroimaging and Data Science (TReNDS), Georgia State University, Georgia Institute of Technology, Emory University, Atlanta, Georgia, USA;
4. Departments of Psychology and Computer Science, Georgia State University, Atlanta, USA;
5. Department of Electrical and Computer Engineering, Georgia Institute of Technology, Atlanta, USA;
6. Neurophysiology Unit, Azienda Socio Sanitaria Territoriale Spedali Civili Brescia, Brescia, Italy;
7. Neuroradiology Unit, University of Brescia, Brescia, Italy;
8. Laboratory Unit, Azienda Socio Sanitaria Territoriale Spedali Civili Brescia, Brescia, Italy;
9. Department of Neurodegenerative Disease, Dementia Research Centre, UCL Institute of Neurology, Queen Square, London
10. Department of Neurology,Erasmus Medical Centre, Rotterdam, Netherlands;
11. Alzheimer's disease and Other Cognitive Disorders Unit, Neurology Service, Hospital Clinic, University of Barcelona, Barcelona, Spain;
12. Cognitive Disorders Unit, Department of Neurology, Donostia University Hospital, San Sebastian, Gipuzkoa, Spain;
13. Clinique Interdisciplinaire de Memoire, Department des Sciences Neurologiques, CHU de Quebec, and Faculte de Medecine, Universite Laval, QC, Canada;
14. Center for Alzheimer Research, Division of Neurogeriatrics, Department of Neurobiology, Care Sciences and Society, Bioclinicum, Karolinska Institutet, Solna, Sweden;
15. Department of Neurodegenerative Diseases, Hertie-Institute for Clinical Brain Research and Center of Neurology, University of Tubingen, Tubingen, Germany;
16. Fondazione Ca' Granda, IRCCS Ospedale Policlinico, Milan, Italy;
17. University of Milan, Centro Dino Ferrari, Milan, Italy;
18. Department of Clinical Neurosciences, University of Cambridge, Cambridge, UK;

19. Sunnybrook Health Sciences Centre, Sunnybrook Research Institute, University of Toronto, Toronto, Canada;
20. Tanz Centre for Research in Neurodegenerative Diseases, University of Toronto, Toronto, Canada;
21. Department of Clinical Neurological Sciences, University of Western Ontario, London, Ontario Canada;
22. Laboratory for Cognitive Neurology, Department of Neurosciences, KU Leuven, Leuven, Belgium;
23. Neurology Service, University Hospitals Leuven, Leuven, Belgium;
24. Leuven Brain Institute, KU Leuven, Leuven, Belgium;
25. Laboratory of Neurosciences, Institute of Molecular Medicine, Faculty of Medicine, University of Lisbon, Lisbon, Portugal;
26. Fondazione IRCCS Istituto Neurologico Carlo Besta, Milano, Italy;
27. Nueld Department of Clinical Neurosciences, Medical Sciences Division, University of Oxford, Oxford, UK;
28. University Hospital of Coimbra (HUC), Neurology Service, Faculty of Medicine, University of Coimbra, Coimbra, Portugal;
29. Division of Neuroscience and Experimental Psychology, Wolfson Molecular Imaging Centre, University of Manchester, Manchester, UK;
30. Sorbonne Université, Paris Brain Institute – Institut du Cerveau – ICM, Inserm U1127, CNRS UMR 7225, AP-HP - Hôpital Pitié-Salpêtrière, Paris, France;
31. Centre de référence des démences rares ou précoces, IM2A, Département de Neurologie, AP-HP - Hôpital Pitié-Salpêtrière, Paris, France;
32. Département de Neurologie, AP-HP - Hôpital Pitié-Salpêtrière, Paris, France;
33. Reference Network for Rare Neurological Diseases (ERN-RND);
34. Department of Psychiatry, McGill University Health Centre, McGill University, Montreal, Quebec, Canada;
35. Neurologische Klinik, Ludwig-Maximilians-Universitat Munchen, Munich, Germany;
36. Department of Neurology, University of Ulm, Ulm, Germany;
37. Department of Neurofarba, University of Florence, Italy;
38. IRCCS Fondazione Don Carlo Gnocchi, Florence, Italy;

^ see appendix for consortium authors

*Corresponding author:
Barbara Borroni, MD
Clinica Neurologica, Università degli Studi di Brescia
P.le Spedali Civili 1, 25123, Brescia, Italy
Phone: 0039 0303995632
Email: bborroni@inwind.it

Title character count: 113
Number of references: 46
Number of tables: 2

Number of figures: 3
Abstract word count: 297
Main text word count: 4816

Abstract

Background: The presymptomatic brain changes of *granulin (GRN)* disease, preceding by years frontotemporal dementia (FTD), has not been fully characterized. New approaches focus on the spatial chronnectome can capture both spatial network configurations and their dynamic changes over time.

Objective: To investigate the spatial dynamics in 141 presymptomatic *GRN* mutation carriers and 282 non-carriers from the Genetic Frontotemporal dementia research Initiative (GENFI) cohort.

Methods: We considered time-varying patterns of the default mode network, the language network, and the salience network, each summarized into four distinct recurring spatial configurations. Dwell time (DT) (the time each individual spends in each spatial state of each network), fractional occupacy (FO) (the total percentage of time spent by each individual in a state of a specific network) and total transition number (TN) (the total number of transitions performed by each individual in a specifict state) were considered. Correlations between DT, FO and TN and estimated years from expected symptom onset (EYO) and clinical performances were assessed.

Results: Presymptomatic *GRN* mutation carriers spent significantly more time in those spatial states characterised by greater activation of the insula and the parietal cortices, as compared to non-carriers ($p<0.05$, FDR-corrected). A significant correlation between DT and FO of these spatial states and EYO was found, the longer the time spent in the spatial states, the closer the EYO. DT and FO significantly correlated with performances at tests tapping processing speed, with worse scores associated with increased spatial states' DT.

Conclusion: Our results demonstrated that presymptomatic *GRN* disease presents a complex dynamic reorganization of brain connectivity. Change in both the spatial and temporal aspects of

brain network connectivity could provide a unique glimpse into brain function and potentially allowing a more sophisticated evaluation of the earliest disease changes and the understanding of possible mechanisms in *GRN* disease.

Introduction

Frontotemporal dementia (FTD) is a clinical and neuropathological heterogeneous disorder, characterized by language impairment, deficits in executive functions, and behavioural and/or personality disturbances (Gorno-Tempini et al., 2011; Rascovsky et al., 2011).

Pathogenetic mutations within the granulin (*GRN*) gene, one of the most common causes of familial FTD with TAR-DNA binding protein 43 (TDP-43) inclusions (Baker et al., 2006; Cruts et al., 2006), mostly present with behavioral variant FTD or non-fluent primary progressive aphasia (Moore et al., 2020). Clinical symptoms are preceded by a long accrual of subtle changes, which provide a unique time-window to study the earliest disease stages. (Chitramuthu et al., 2017; Panman et al., 2021). In particular, the study of preclinical brain changes might give novel insights into the pathophysiological processes, and into potential compensatory mechanisms occurring before the onset of symptoms, thus representing potential targets of intervention.

Only a few resting-state functional magnetic resonance imaging (MRI) connectivity studies are available so far, mainly suggesting the impairment of brain connectivity within the salience network (SN) and the default mode network (DMN) (Borroni et al., 2012; Dopper et al., 2013; Feis et al., 2019; Lee et al., 2019; Enrico Premi et al., 2014; E. Premi et al., 2014; Premi et al., 2016). However, these studies hold a common assumption that each brain network is comprised of a fixed set of brain regions with a static spatial pattern over time (i.e., static functional network connectivity, sFNC) (Iraji et al., 2019a). This is indeed an oversimplification, as the resting brain is highly dynamic, with reoccurring variation in spatial patterns of brain functional organization during time (Calhoun et al., 2014; A Iraji et al., 2020).

As such, while previous studies have focused on capturing dynamic brain network connectivity by assessing the variations in the temporal coupling between spatially static brain networks (Abrol et al., 2017; Allen et al., 2014; Calhoun et al., 2014; Armin Iraji et al., 2020; Miller et al., 2016),

recent studies have explored the possibility to capture time-varying spatial patterns of brain networks (Iraji et al., 2019a, 2019b). In other words, functional brain networks are only transiently isolated, and each brain network may assume different configurations in space (i.e., "dissemination in space") during the scan period (i.e., "dissemination in time") (A Iraji et al., 2020). This results in a number of identifiable spatial states, that may recruit distinct neuroanatomical brain regions, for each considered functional brain network (i.e. DMN or the SN). It is worth noting that spatial chronnectome focuses on variations in the spatial pattern of a given network (e.g., DMN) and leverages the spatial information to capture brain dynamics. This differs from performing dynamic functional network connectivity analysis on the subnetworks of a given network (e.g., evaluating dynamic functional network connectivity between subnetworks of DMN obtained from high model order ICA), which studies time-varying properties of the temporal couplings between subnetworks activity patterns (i.e., no spatial information is included in studying brain dynamics) (A Iraji et al., 2020; Iraji et al., 2019a).

In this view, a spatial chronnectome analysis may enable a more sophisticated evaluation of the spontaneously fluctuating nature of neuronal signals by assessing both spatial network configurations and their dynamic changes over time. Moreover, a spatial chronnectome analysis might be able to detect patterns of brain reorganization in the earliest phases of FTD pathology. Therefore, the goal of the present study is to investigate whether the spatial chronnectome approach may reveal the early dynamic changes in presymptomatic FTD. To this, we considered presymptomatic subjects with *GRN* mutations from the Genetic Frontotemporal dementia Initiative (GENFI) (www.genfi.org) (Rohrer et al., 2015).

Methods

Participants. Data for this study were drawn from the GENFI 2 multicentre cohort study (data freeze 5), which consists of 26 research centres across Europe and Canada (www.genfi.org.uk). Inclusion and exclusion criteria have been previously described (Rohrer et al., 2015). Local ethics committees approved the study at each site, and all participants provided written informed consent according to the Declaration of Helsinki.

For the aim of the present work, we considered subjects carrying a pathogenic mutation within the *GRN* gene and, as control group, their first-degree relatives not carrying pathogenetic *GRN* mutations, for whom an MRI scan acquired on a 3T scanner was available.

Estimated years from expected symptom onset in presymptomatic *GRN* mutation carriers were calculated as the age of the participant at the time of the study assessment minus the mean familial age at symptom onset, as previously reported (Rohrer et al., 2015). Each subject underwent a standardised neuropsychological assessment, as previously reported (Rohrer et al., 2015).

MRI acquisition. MRI protocol was common to all the GENFI sites and adapted for different scanners; no pre-study phantom harmonization was performed at local level. In summary, T2-weighted echo planar imaging (EPI) sequences sensitized to blood oxygenation level dependent (BOLD) contrast for rs-fMRI were considered in the present study (Premi et al., 2019). As the volume numbers (ranging from 140 to 200) varied across the GENFI centres, we considered only the first 140 volumes of the EPI images for each subject. In particular, we had 369 subjects with 200 timepoints that were cropped to 140, discharging the last 60 timepoints (mean acquisition time: 326.22 ± 20.54 sec). From this point of view, Furthermore, differences in repetition times (TRs, ranging from 2200 ms to 2500 ms) (see **Supplementary Table 1**) has been considered in spatial

chronnectome preprocessing and analysis. During scanning, subjects were asked to keep their eyes closed, not to think of anything in particular, and not to fall asleep.

Neuroimaging pre-processing and analyses. Functional data were pre-processed using the toolbox for Data Processing & Analysis for Brain Imaging (DPABI, http://rfmri.org/dpabi) (Yan et al., 2016) based on the Statistical Parametric Mapping (SPM12, https://www.fil.ion.ucl.ac.uk/spm/) software. For each subject, the first two volumes of the fMRI series were discharged to account for magnetization equilibration. The remaining 138 volumes underwent slice-timing correction and were realigned to the first volume. Any subject who had a maximum displacement in any direction larger than 2.5 mm, or a maximum rotation (x,y,z) larger than 2.5°, was excluded. We considered framewise displacement (FD) (Power et al., 2012) as a nuisance variable accounting for head motion during MRI scanning. Data were subsequently spatially normalized to the EPI unified segmentation template (considering that EPI normalization is able to reduce variability across subjects) (Calhoun et al., 2017) in Montreal Neurological Institute coordinates derived from SPM12 software and resampled to 3x3x3 cubic voxels. Spatial smoothing with an isotropic Gaussian kernel with the full width at half-maximum of 6 mm was applied, followed pre-processing pipeline previously adopted for spatial chronnectome analysis (Iraji et al., 2019a).

Functional Networks Decomposition. The functional imaging data were processed using the GIFT (GIFT toolbox, http://trendscenter.org/software/gift), and a spatially constrained multivariate objective optimization ICA with reference (MOO-ICAR) (Du et al., 2015; Du and Fan, 2013) was used to obtain spatial maps for selected large-scale networks, namely the default mode network (DMN), the language network (LN) and the salience network (SN), from a recently published set of brain networks (Iraji et al., 2019a). Spatial maps are used as reference templates to calculate

functional networks for each subject by maximizing independence in the context of the spatial constraint. These template maps include the brain networks with a not-artefactual neuronal origin and assign the remaining data to be noise. We have taken advantage of the recently published set of 12 spatial maps for our network selection, considering DMN, LN and SN as network of interest (Iraji et al., 2019a). The TR of each subject was entered in GIFT pre-processing, and we accounted for TR values differences among centres (143 subjects with TR=2200 ms, 280 subjects with TR=2500 ms) interpolating the data to the minimum TR (2200 ms).

These processed data were also used for sFNC statistical analysis, considering the DMN, LN, and SN large-scale networks derived from MOO-ICAR pre-processing analysis (see **Supplementary Figure, panel A**), as well as for spatial chronnectome analysis.

Dynamic coupling maps calculation (dCM), k-means clustering, dwell time (DT), fractional occupacy (FO) and total transitions number (TN) calculation. The spatial chronnectome analysis was achieved using the dynamic FNC toolbox implemented in GIFT (GIFT toolbox, http://trendscenter.org/software/gift). Sliding window length or number of clusters were chosen according to previous literature data on dynamic connectivity (Armin Iraji et al., 2020; Iraji et al., 2019a). The single time courses were detrended (to remove baseline drifts from the scanners and/or physiological pulsations), orthogonalized with respect to 12-motion parameters, despiked (replacement of outlier time points with 3rd order spline fitting to clean neighbouring points) and filtered using a 5th order Butterworth filter (0.01 to 0.15 Hz). For each considered brain network, the temporal coupling between a specific brain network and every voxel of the brain was calculated using the sliding-window correlation approach resulting in one dCM per window. This procedure takes all the potential associations into account and fully captures the relationship between each voxel and the brain network (for example, if a given voxel is highly correlated with two networks,

correlation analysis allows the detection of both of these associations). We used the tapered window obtained by convolving a rectangle (width = 30 TRs) with a Gaussian (σ = 3 TRs) and the sliding step size of one TR resulting in 108 windows per subject (Armin Iraji et al., 2020; Iraji et al., 2019a).

k-means clustering was applied to summarize the dCMs of each brain network into a set of spatial states , which allows us to investigate the dynamic properties of the brain network via temporal variations of these distinct spatial states. The number of spatial states was set to 4, in line with Iraji et al. (Iraji et al., 2019a). For each brain network, *k*-means clustering was applied on the 45684 (423 subjects × 108 windows) dCMs of the brain network. *K*-means clustering was repeated 100 times with different initializations using the *k*-means++ technique to increase the chances of escaping local minima (Arthur and Vassilvitskii, 2007). The correlation distance metric was used to measure the similarity between data points (i.e., the dCMs), as it is more effective in the detection of spatial patterns irrespective of voxel intensities. Using temporal profiles of the spatial states, the mean dwell time (DT), *i.e.* the average of the amount of time that subjects stay in a given state once entering that state), the fractional occupacy (FO), *i.e.* the total percentage of time that subjects spent in a given state, and the total transition number (TN), *i.e.* the total number of transitions among states performed by subjects for each network, were calculated for each network, as state-level dynamic indexes to summarize dynamic properties of each network.

Static Functional Network Connectivity (sFNC) analysis. MOO-ICAR preprocessing was used a to estimate individual networks (Iraji et al., 2019a). Back-reconstruction step considered the estimation of subject-specific networks and their related time courses based on the selected 3 networks (DMN, LN and SN) (Iraji et al., 2019a; Salman et al., 2019). Statistical analysis was then performed using SPM12, as follows: *a)* between-group comparison (presymptomatic *GRN* carriers

vs healthy controls), considering age, gender, site, FD Powers and insular volume (as % of TIV) as nuisance variables ($p<0.001$ uncorrected for multiple comparisons and $p<0.05$ family-wise error whole-brain); *b)* multiple regression to assess the relationship between imaging variables and age at expected symptom onset (EYO) or neuropsychological tests, covarying for gender, age, FD Powers, site and insular volume (as % of TIV), as appropriate ($p<0.001$ uncorrected for multiple comparisons and $p<0.05$ FWE whole-brain).

Furthermore, on the whole group of subjects (presymptomatic *GRN* carriers and healthy controls) brain connectome was calculated to assess betwee-network connectivity. A connectogram was reported to show the correlations among considered networks (DMN, LN and SN) using bezier curves and thumbnails of spatial maps.

Statistical analyses. Comparisons of demographic and clinical characteristics were assessed by Student's t-test for continuous variables and χ^2 test for categorical variables.

A univariate general linear model (GLM) was adopted to study the main effect of group (*GRN* vs HC) considering age, gender, FD, site and insular volume (as % of total intracranial volume [TIV]) as nuisance variables, and corrected for multiple comparisons (Benjamini and Hochberg, 1995).

Partial correlation analyses were used to assess the relationship between imaging variables and age at expected symptom onset (EYO) or neuropsychological tests, covarying for gender, age, FD Powers, site and insular volume (as % of TIV), as appropriate. A multiple stepwise regression analysis was run to predict EYO from gender, site, FD Powers, insular volume (as % of TIV) and dynamic indexes (separated analyses were performed for DT and FO) significantly correlated with EYO in partial correlation analysis.

All the statistical analysis was performed using IBM SPSS Statistics 22.0 (Chicago, USA) and statistical significance level set at $p<0.05$.

Results

Participants.

Four-hundred twenty-three participants were included in the present study, namely 141 with a pathogenic mutation in the *GRN* gene (age = 45.9 ± 11.9 years, female = 63.8%) and 282 non-carrier first-degree relatives, who therefore acted as controls within the study (age = 46.5 ± 13.2 years, female = 57.4%) (see **Table 1** for demographic and clinical characteristics).

Assessing the spatial chronnectome.

We first assessed time-varying information of each brain network into spatial patterns, termed spatial states, in the whole group of participants. For each brain network, we identified four distinct spatial states (from 1 to 4). Each spatial state consists of a hub, expected to be part of the referral network all the time, and other brain regions that selectively differentiate the brain network in the different spatial states. Additionally, anti-correlative connections may be identified in different segments of time in each spatial state, further underlying the existence of extra regions associated with specific networks at different moments in time.

For the purpose of the present study, we focused on the spatial dynamics within the DMN, the LN, and the SN, mainly involved in FTD pathology.

Default mode network (DMN). As previously demonstrated (Iraji et al., 2019a), each of the four spatial states of the DMN are defined by posterior cingulate cortex hub, with spatial state 1 representing the "classical" already described DMN with the frontal cortex hub, that was substantially reduced in spatial state 2 (see **Figure 1** hot colour); moreover, spatial state 2 presents anti-correlative connections with the insula (see **Figure 1** cold colours). The spatial state 3 of DMN is characterised by reduced activation of posterior cingulate cortex hub and the lack of frontal

region activation, as compared to "classical" DMN, while sensorimotor and occipital areas anticorrelated to DMN in spatial state 4 (see **Figure 1** cold colours).

Language network (LN). The LN is overall characterised by parietal and posterior cingulate hub, bilaterally, clearly depicted in spatial state 1. Spatial state 2 is defined by greater temporo-parietal network activation and selective temporal pole activation along with anti-correlative connections with the bilateral frontal cortex; a more pronounced activation of the parietal and posterior cingulate hub represents spatial state 3, while an even more pronounced bilateral activation of temporo-parietal hub is the signature of spatial state 4 (see **Figure 2**).

Salience network (SN). The four spatial states of the SN are characterized by the frontal hub, with more pronounced signal in the insula region, bilaterally, in spatial state 1, and with anti-correlative connections with DMN regions in spatial state 1, 3 and 4 and with anti-correlative connections within medial frontal regions in spatial state 3 and 4. Notably, anti-correlation with DMN was more pronouced in spatial state 4. Spatial state 2 is characterised by "classical" already described SN, with no extra regions of co-activation (see **Figure 3**).

Dwell time (DT), fractional occupacy (FO) and total transitions number (TN) in presymptomatic *GRN* mutation carriers as compared to HC.

We therefore analysed DT, FO and TN, for each of the considered networks, in presymptomatic *GRN* as compared to HC. The mean DTs in *GRN* and HC groups are reported in **Table 2**, whereas FO and TN mean values are reported in **Supplementary Table 1**.

Default mode network (DMN). When we considered DMN, presymptomatic *GRN* mutation carriers spent more time (DT) in spatial state 2, namely the spatial state with anti-correlative connections with the insula bilaterally ($p<0.05$, FDR-corrected, see **Figure 1**). Furthermore, considering FO,

presymptomatic *GRN* carriers stayed for a lesser extent in spatial state 4 (FO) ($p<0.05$, FDR-corrected, see **Supplementary Table 2**). We did not find any significant differences in NT.

Language network (LN). When we considered LN, presymptomatic *GRN* mutation carriers spent more time (DT and FO) in spatial state 4, the spatial state with the more pronounced activation of the parietal hub and lacking the temporal pole activation ($p<0.05$, FDR-corrected, see **Figure 2** and **Supplementary Figure 1**). Moreover, limited to FO, presymptomatic *GRN* carriers spent less time in spatial state 2 ($p<0.05$, FDR-corrected, see **Supplementary Table 2**). We did not find any significant differences in NT.

Salience network (SN). When we considered the SN, *GRN* mutation carriers spent more time (DT and FO) in spatial state 1, the one with the most pronounced activation of the insula region, and less time (DT and FO) in spatial state 4, one of the states associated with anti-correlative connections within regions belonging to DMN (frontal, parietal regions bilaterally, posterior cingulate cortex), as compared to HC ($p<0.05$, FDR-corrected, see **Figure 3** and **Supplementary Figure 1**).

Correlation between estimated years from expected symptom onset (EYO) and dwell time (DT), fractional occupacy (FO) and total transitions number (TN) in *GRN* mutations carriers. Correlation between DT, FO and NT of spatial states and EYO was analysed. For DT, we found significant correlations between *a)* DT of DMN spatial state 2 and EYO, the longer the time spent in DMN spatial state 2, the closer the disease onset ($r = 0.236$, $p < 0.05$ FDR-corrected), *b)* DT of LN spatial state 3 and EYO, the longer the time spent in LN spatial state 3 the further the disease onset ($r=-0.190$ $p<0.05$ FDR-corrected) and, *c)* DT of LN spatial state 4 and EYO, the longer the time spent in LN spatial state 4, the closer the disease onset ($r=0.286$ $p<0.05$ FDR-corrected). No significant association between DT and EYO for SN spatial states was observed. Regression analyses identified

LN spatial state 4 (B=0.084, β = 0.214, p = 0.016), as the best predictors of EYO in presymptomatic *GRN* mutation carriers.

When we considered FO, a comparable pattern of correlations were found between *a)* FO of DMN spatial state 2 and EYO (r=0.272, p<0.05 FDR-corrected), *b)* FO of LN spatial state 3 and EYO (r=-0.205 p<0.05 FDR-corrected) and *c)* FO of LN spatial state 4 and EYO (r=0.332 p<0.05 FDR-corrected). No significant association between FO and EYO for SN spatial states was observed. Regression analyses identified LN spatial state 4 (B=8.925, β = 0.236, p = 0.006), as the best predictors of EYO in presymptomatic *GRN* mutation carriers.

To further elucidate the role of LN state 4 in predicting EYO, regression analysis demonstrated that an increase in DT of one second was associated with a closer clinical onset equal to one month (B=0.084, 30.66 days). Moreover, setting a cut-off value of DT equal to 60 seconds (for details see **Supplementary Figure 2**), *GRN* carriers with higher values (18 subjects, mean value=97.3±15.7 seconds) vs *GRN* carriers with lower values (123 subjects, mean value=14.4±13.6 seconds) showed a significantly different EYO (-6.9±9.2 years vs. -15.1±12.2 years, p=0.02, applying univariate GLM corrected for gender, site, FD Powers and insular volume as nuisance variables).

Correlation between neuropsychological assessment and dwell time (DT), fractional occupacy (FO) and total transitions number (TN) in *GRN* mutations carriers.

To further explore the correlation between DT, FO, NT and cognitive performances, we considered tests demonstrated to be altered already before EYO 23, tapping executive functions and processing speed (Trail Making Test, part A and B) and naming (Boston Naming Test) (see **Table 1** for mean scores).

A significant correlation was found between DT and FO of SN spatial state 1 and TMT part A (r=0.235 and r=0.286, respectively, both p=0.05 FDR-corrected), the longer the time spent in SN

spatial state 1 the worse the score at TMT. For DMN spatial state 2, a significant correlation between FO and TMT part A was reported (r=0.256, p=0.05 FDR-corrected).

No significant correlations with the remaining neuropsychological tests were found. Moreover, no significant findings for TN were reported.

Static functional network connectivity - sFNC.

When sFNC was assessed, the brain connectome (connectogram) showed a significant negative correlation between DMN and SN in the whole group of subjects, and with a lesser extent, a negative correlation between SN and LN and a positive correlation between LN and DMN (**Supplementary Figure 3, Panel B**).

Within-network connectivity (between presymptomatic *GRN* carriers and healthy controls) of the three considered networks (DMN, LN and SN) (**Supplementary Figure 3, Panel A**) showed no significant differences at the pre-established thresholds ($p<0.001$ uncorrected). Moreover, multiple regression analyses (to assess the potential relationship between sFNC and EYO as well as with cognitive performances) did not show any statistically significant cluster at the pre-established threshold ($p<0.001$ uncorrected).

Discussion

The presymptomatic phase of neurodegenerative diseases lasts many years, with progressive modifications and potential compensative mechanisms potentially counteracting the ongoing pathological process. In the present study, we have examined the earliest brain changes in subjects with highly penetrant *GRN* mutations, and we have demonstrated a complex and dynamic network reorganization occurring before the onset of clinical symptoms.

We conducted a three steps study design: *a)* firstly, we selected three networks of interest, namely the SN and the LN, as *GRN*-related disease usually presents with behavioural variant FTD or non-fluent primary progressive aphasia (Gorno-Tempini et al., 2011; Rascovsky et al., 2011), and the DMN, as previously demonstrated to be involved in FTD (Borroni et al., 2012; Lee et al., 2019; Zhou et al., 2010); *b)* we applied an advanced spatial chronnectome approach (Iraji et al., 2019a), that allowed us to evaluate not only static FNC (i.e., SN, LN, DMN) but also to assess the distinct conformational spatial states of each individual network and their dynamic patterns over time (i.e., spatial state 1-4); and *c)* we computed mean dwell times for each considered network, namely the time each subject spends in each spatial state, in *GRN* mutation carriers *vs* non-carriers.

One of the two main findings of the present study is that, in presymptomatic disease stage, *GRN* mutation carriers significantly spend more time in those spatial states characterised by activation of cortical regions that will be involved in the symptomatic stages of disease (Rohrer et al., 2015). As compared to controls, *GRN* mutation carriers spent more time in spatial state 4 of the LN, characterised by greater activation of parietal cortex, as compared to the other spatial states of the LN, and in spatial state 1 of the SN, characterised by greater activation of the insula, as compared to the other spatial states of the SN. Indeed, it might be argued that the selective or the main involvement of either insula or parietal regions might drive the development of clinical phenotype, namely behavioural variant FTD or non-fluent primary progressive aphasia.

Conversely, in line with previous literature data (Borroni et al., 2012; Dopper et al., 2013; Feis et al., 2019; Lee et al., 2019; Enrico Premi et al., 2014; E. Premi et al., 2014; Premi et al., 2016), the analysis of sFNC between *GRN* mutation carriers and healthy controls did not yield any significant result. The lack of significant results of sFNC is somehow not surprising as it considers the mean overall rs-MRI signal of each network, in a disease stage with substantial absence of structural brain changes (Borrego-Écija et al., 2021).

The second main result of the present work is that the dynamic interplay between DMN and SN shows substantial changes in the presymptomatic stages of *GRN* disease. We reported that *GRN* mutation carriers spent more time in DMN spatial state 2, where DMN is anticorrelated with bilateral insular regions belonging to SN, and spent less time in SN spatial state 4, where SN is anticorrelated with all the nodes belonging to DMN, with an imbalance of the physiological relationship between DMN and SN.

Literature data on static between-networks' connectivity (connectogram) (Allen et al., 2011; Fox et al., 2005; Uddin et al., 2009) (as well as the present work, Supplementary Figure 1B) have already demonstrated the presence of significant negative correlations (anticorrelations) between SN and DMN, with an antagonistic interaction during social and self-related cognitive activities (Seeley et al., 2007).

Indeed, the present analysis, allowing the identification of regions not primarily belonging to the referral hub of the network, suggests a paradoxical behaviour of presymptomatic *GRN* disease with a widespread whole-brain connectivity breakdown of at-distance brain networks and derangement of the competitive relationships between SN and DMN (Tognoli and Kelso, 2014). Once again, *GRN* mutation carriers spent more time in those networks with greater engagement of regions involved in symptomatic disease, i.e., regions belonging to the SN and the insula.

The ability to measure the intrinsic functional architecture of the brain has grown exponentially over the last two decades (White and Calhoun, 2019). The assumption at the basis of spatial chronnectome is that connections within the brain can differentially fire between different regions at different times, and these differences can be quantified (Saha et al., 2021). Indeed, this is the first study assessing spatial chronnectome in presymptomatic monogenic FTD and in preclinical dementia in general, thus whether network dynamic connectivity reorganization acted to increase brain efficiency or is an early feature of Granulin haploinsufficiency is yet to be clarified (Lee et al., 2019). However, changes within the insula and parietal cortex have been described as the earliest signature of *GRN* disease (Cash et al., 2018; Lee et al., 2019; Panman et al., 2021; Rohrer et al., 2015), suggesting that the selective activation of functional connectivity of these brain regions might contribute to the maintenance of cognitive functions. The significant relationship between estimated years from expected symptom onset and spatial states' dwell times further strength this hypothesis, the closer the onset of symptoms the longer the time spent in the spatial states with increased insula and parietal cortex connectivity (*i.e.,* DMN spatial state 2 and LN spatial state 4); on the other side, the further estimated years from expected symptom onset were associated with longer time spent in spatial states resembling the "classical" hubs, with no anti-correlative extra-regions activation within the insula (*i.e.,* DMN spatial state 3) and less activation of parietal cortex (*i.e.,* LN spatial state 1).

Furthermore, TMT-A (Bowie and Harvey, 2006), directly correlated with the time spent in SN spatial state 1. As an index of pre-processing speed skill, TMT-A is one of the early cognitive markers in preclinical FTD (Rohrer et al., 2015). The absence of a significant correlation between TMT-A scores and meta-state measures in healthy controls further supports the idea that this finding is not age-driven but mutation-driven (data not shown).

The current study has a number of limitations. First, we considered only *GRN* mutations and the assessment and comparison with other monogenic FTD disorders should be considered in future work as well as the effect of different mutations within the same gene and the heterogeneity of clinical phenotypes. In addition, our analysis included the estimated age at onset, but we recognize that possible biases and possible discrepancies across mutations and families may occur (Moore et al., 2020). Moreover, we recognize possible variance in acquisition protocols in this multi-site neuroimaging study, even though a careful harmonization of sequences and data was carried out to reduce differences across scanning platforms. In particular, unstable wakefulness with the tendency to drift into sleep can affect fMRI acquisition (Tagliazucchi and Laufs, 2014; Wang et al., 2017). Recently, arousal fluctuation were linked to global waves of activity propagating throughout the brain, potentially contributing to fMRI signal fluctuations (Raut et al., 2021). From this point of view, even if an objective measurement of arousal fluctuation was not available for our sample, during MRI site harmonization the majority of subjects (<85%) were cropped to 140 timepoint (as described in details in Methods section), discharging the last 60 timepoints (that can be considered as the most critical part of fMRI acquisition with regard to arousal problems) (Allen et al., 2018; Damaraju et al., 2020; Tagliazucchi and Laufs, 2014; Wang et al., 2017). Finally, still unresolved issues regarding the application of dynamic functional connectivity analyses to resting fMRI data may limit the insights that can be gained from this promising new research area (Lurie et al., 2020). In conclusion, presymptomatic *GRN* disease presents a complex perturbation of spatial chronnectome, detectable at whole-brain and at a network-level, despite the absence of sFNC abnormalities. Presymptomatic *GRN* disease spent more time in those networks primarily affected by earliest neuropathological changes (Gass et al., 2006) and presented an imbalance of the physiological competitive relationship between the DMN and the SN. Spatial chronnectome, evaluating both the spatial and temporal changes of brain network connectivity, provides a more

sophisticated evaluation of the earliest disease changes leading to disease onset, and may help in understanding the possible causative mechanisms in *GRN* disease.

Acknowledgements

We thank our participant volunteers and their families for their participation; the radiographers/technologists and research nurses from all centers involved in this study for their invaluable support in data acquisition.

Funding

This work is supported by JPND grant "GENFI-prox" (to MS, JvS, MO, CG, JR, and BB), the Centre d'Investigation Clinique (ICM, France), the Centre pour l'Acquisition et le Traitement des Images platform (CATI, France), the UK Medical Research Council, and the Canadian Institutes of Health Research as part of a Centres of Excellence in Neurodegeneration grant, a Canadian Institutes of Health Research operating grant, Fundació Marató de TV3, Spain.

Appendix – GENFI consortium

- **Sónia Afonso** Instituto Ciencias Nucleares Aplicadas a Saude, Universidade de Coimbra, Coimbra, Portugal
- **Maria Rosario Almeida** Faculty of Medicine, University of Coimbra, Coimbra, Portugal
- Sarah Anderl-Straub Department of Neurology, University of Ulm, Ulm, Germany
- **Christin Andersson** Department of Clinical Neuroscience, Karolinska Institutet, Stockholm, Sweden
- **Anna Antonell** Alzheimer's disease and Other Cognitive Disorders Unit, Neurology Service, Hospital Clínic Barcelona, Spain
- **Andrea Arighi** Fondazione IRCCS Ca' Granda Ospedale Maggiore Policlinico, Neurodegenerative Diseases Unit, Milan, Italy; University of Milan, Centro Dino Ferrari, Milan, Italy
- **Mircea Balasa** Alzheimer's disease and Other Cognitive Disorders Unit, Neurology Service, Hospital Clínic, Barcelona, Spain
- **Myriam Barandiaran** Cognitive Disorders Unit, Department of Neurology, Donostia University Hospital, San Sebastian, Gipuzkoa, Spain; Neuroscience Area, Biodonostia Health Research Insitute, San Sebastian, Gipuzkoa, Spain
- **Nuria Bargalló** Imaging Diagnostic Center, Hospital Clínic, Barcelona, Spain
- **Robart Bartha** Department of Medical Biophysics, The University of Western Ontario, London, Ontario, Canada; Centre for Functional and Metabolic Mapping, Robarts Research Institute, The University of Western Ontario, London, Ontario, Canada
- **Benjamin Bender** Department of Diagnostic and Interventional Neuroradiology, University of Tübingen, Tübingen, Germany
- **Maxime Bertoux** Inserm 1172, Lille, France
- **Anne Bertrand** Sorbonne Université, Paris Brain Institute – Institut du Cerveau – ICM, Inserm U1127, CNRS UMR 7225, AP-HP - Hôpital Pitié-Salpêtrière, Paris, France
- **Valentina Bessi** Department of Neuroscience, Psychology, Drug Research and Child Health, University of Florence, Florence, Italy
- **Sandra Black** Sunnybrook Health Sciences Centre, Sunnybrook Research Institute, University of Toronto, Toronto, Canada
- **Sergi Borrego-Ecija** Alzheimer's disease and Other Cognitive Disorders Unit, Neurology Service, Hospital Clínic, Barcelona, Spain
- **Arabella Bouzigues** Department of Neurodegenerative Disease, Dementia Research Centre, UCL Institute of Neurology, Queen Square, London, UK
- **Jose Bras** Center for Neurodegenerative Science, Van Andel Institute, Grand Rapids, Michigan, MI 49503, USA
- **Alexis Brice** Sorbonne Université, Paris Brain Institute – Institut du Cerveau – ICM, Inserm U1127, CNRS UMR 7225, AP-HP - Hôpital Pitié-Salpêtrière, Paris, France
- **Rose Bruffaerts** Laboratory for Cognitive Neurology, Department of Neurosciences, KU Leuven, Leuven, Belgium
- **Agnès Camuzat** Sorbonne Université, Paris Brain Institute – Institut du Cerveau – ICM, Inserm U1127, CNRS UMR 7225, AP-HP - Hôpital Pitié-Salpêtrière, Paris, France
- **Marta Cañada** CITA Alzheimer, San Sebastian, Gipuzkoa, Spain
- **Valentina Cantoni** Centre for Neurodegenerative Disorders, University of Brescia, Brescia, Italy
- **Paola Caroppo** Fondazione IRCCS Istituto Neurologico Carlo Besta, Milano, Italy
- **Miguel Castelo-Branco** Faculty of Medicine, University of Coimbra, Coimbra, Portugal
- **Olivier Colliot** Sorbonne Université, Paris Brain Institute – Institut du Cerveau – ICM, Inserm U1127, CNRS UMR 7225, AP-HP - Hôpital Pitié-Salpêtrière, Paris, France
- **Thomas Cope** Department of Clinical Neuroscience, University of Cambridge, Cambridge, UK
- **Vincent Deramecourt** Univ Lille, France
- **Giuseppe Di Fede** Fondazione IRCCS Istituto Neurologico Carlo Besta, Milano, Italy
- **Alina Díez** Neuroscience Area, Biodonostia Health Research Insitute, San Sebastian, Gipuzkoa, Spain
- **Diana Duro** Faculty of Medicine, University of Coimbra, Coimbra, Portugal

- **Chiara Fenoglio** Fondazione IRCCS Ca' Granda Ospedale Maggiore Policlinico, Neurodegenerative Diseases Unit, Milan, Italy; University of Milan, Centro Dino Ferrari, Milan, Italy
- **Camilla Ferrari** Department of Neuroscience, Psychology, Drug Research and Child Health, University of Florence, Florence, Italy
- **Catarina B. Ferreira** Laboratory of Neurosciences, Institute of Molecular Medicine, Faculty of Medicine, University of Lisbon, Lisbon, Portugal
- **Nick Fox** Department of Neurodegenerative Disease, Dementia Research Centre, UCL Institute of Neurology, Queen Square, London, UK
- **Morris Freedman** Baycrest Health Sciences, Rotman Research Institute, University of Toronto, Toronto, Canada
- **Giorgio Fumagalli** Fondazione IRCCS Ca' Granda Ospedale Maggiore Policlinico, Neurodegenerative Diseases Unit, Milan, Italy; University of Milan, Centro Dino Ferrari, Milan, Italy
- **Aurélie Funkiewiez** Centre de référence des démences rares ou précoces, IM2A, Département de Neurologie, AP-HP - Hôpital Pitié-Salpêtrière, Paris, France
- **Alazne Gabilondo** Neuroscience Area, Biodonostia Health Research Insitute, San Sebastian, Gipuzkoa, Spain
- **Serge Gauthier** Alzheimer Disease Research Unit, McGill Centre for Studies in Aging, Department of Neurology & Neurosurgery, McGill University, Montreal, Québec, Canada
- **Giorgio Giaccone** Fondazione IRCCS Istituto Neurologico Carlo Besta, Milano, Italy
- **Ana Gorostidi** Neuroscience Area, Biodonostia Health Research Insitute, San Sebastian, Gipuzkoa, Spain
- **Caroline Greaves** Department of Neurodegenerative Disease, Dementia Research Centre, UCL Institute of Neurology, Queen Square, London, UK
- **Rita Guerreiro** Center for Neurodegenerative Science, Van Andel Institute, Grand Rapids, Michigan, MI 49503, USA
- **Carolin Heller** Department of Neurodegenerative Disease, Dementia Research Centre, UCL Institute of Neurology, Queen Square, London, UK
- **Tobias Hoegen** Neurologische Klinik, Ludwig-Maximilians-Universität München, Munich, Germany
- **Begoña Indakoetxea** Cognitive Disorders Unit, Department of Neurology, Donostia University Hospital, San Sebastian, Gipuzkoa, Spain; Neuroscience Area, Biodonostia Health Research Insitute, San Sebastian, Gipuzkoa, Spain
- **Vesna Jelic** Division of Clinical Geriatrics, Karolinska Institutet, Stockholm, Sweden
- **Hans-Otto Karnath** Division of Neuropsychology, Hertie-Institute for Clinical Brain Research and Center of Neurology, University of Tübingen, Tübingen, Germany
- **Ron Keren** The University Health Network, Toronto Rehabilitation Institute, Toronto, Canada
- **Gregory Kuchcinski** Univ Lille, France
- **Tobias Langheinrich** Division of Neuroscience and Experimental Psychology, Wolfson Molecular Imaging Centre, University of Manchester, Manchester, UK
- **Thibaud Lebouvier** Univ Lille, France
- **Maria João Leitão** Centre of Neurosciences and Cell Biology, Universidade de Coimbra, Coimbra, Portugal
- **Albert Lladó** Alzheimer's disease and Other Cognitive Disorders Unit, Neurology Service, Hospital Clínic, Barcelona, Spain
- **Gemma Lombardi** Department of Neuroscience, Psychology, Drug Research and Child Health, University of Florence, Florence, Italy
- **Jolina Lombardi** Department of Neurology, University of Ulm, Ulm
- **Sandra Loosli** Neurologische Klinik, Ludwig-Maximilians-Universität München, Munich, Germany
- **Carolina Maruta** Laboratory of Language Research, Centro de Estudos Egas Moniz, Faculty of Medicine, University of Lisbon, Lisbon, Portugal
- **Simon Mead** MRC Prion Unit, Department of Neurodegenerative Disease, UCL Institute of Neurology, Queen Square, London, UK
- **Lieke Meeter** Department of Neurology, Erasmus Medical Center, Rotterdam, Netherlands
- **Gabriel Miltenberger** Faculty of Medicine, University of Lisbon, Lisbon, Portugal

- **Rick van Minkelen** Department of Clinical Genetics, Erasmus Medical Center, Rotterdam, Netherlands
- **Sara Mitchell** Sunnybrook Health Sciences Centre, Sunnybrook Research Institute, University of Toronto, Toronto, Canada
- **Katrina Moore** Department of Neurodegenerative Disease, Dementia Research Centre, UCL Institute of Neurology, Queen Square, London, UK
- **Benedetta Nacmias** Department of Neuroscience, Psychology, Drug Research and Child Health, University of Florence, Florence, Italy
- **Annabel Nelson** Department of Neurodegenerative Disease, Dementia Research Centre, UCL Institute of Neurology, Queen Square, London, UK
- **Jennifer Nicholas** Department of Medical Statistics, London School of Hygiene and Tropical Medicine, London, UK
- **Linn Öijerstedt** Center for Alzheimer Research, Division of Neurogeriatrics, Department of Neurobiology, Care Sciences and Society, Bioclinicum, Karolinska Institutet, Solna, Sweden
- **Jaume Olives** Alzheimer's disease and Other Cognitive Disorders Unit, Neurology Service, Hospital Clínic, Barcelona, Spain
- **Sebastien Ourselin** School of Biomedical Engineering & Imaging Sciences, King's College London, London, UK
- **Jessica Panman** Department of Neurology, Erasmus Medical Center, Rotterdam, Netherlands
- **Janne M. Papma** Department of Neurology, Erasmus Medical Center, Rotterdam, Netherlands
- **Yolande Pijnenburg** Amsterdam University Medical Centre, Amsterdam VUmc, Amsterdam, Netherlands
- **Cristina Polito** Department of Biomedical, Experimental and Clinical Sciences "Mario Serio", Nuclear Medicine Unit, University of Florence, Florence, Italy
- **Sara Prioni** Fondazione IRCCS Istituto Neurologico Carlo Besta, Milano, Italy
- **Catharina Prix** Neurologische Klinik, Ludwig-Maximilians-Universität München, Munich, Germany
- **Rosa Rademakers** Department of Neurosciences, Mayo Clinic, Jacksonville, Florida, USA
- **Veronica Redaelli** Fondazione IRCCS Istituto Neurologico Carlo Besta, Milano, Italy
- **Daisy Rinaldi** Centre de référence des démences rares ou précoces, IM2A, Département de Neurologie, AP-HP - Hôpital Pitié-Salpêtrière, Paris, France
- **Tim Rittman** Department of Clinical Neurosciences, University of Cambridge, Cambridge, UK
- **Ekaterina Rogaeva** Tanz Centre for Research in Neurodegenerative Diseases, University of Toronto, Toronto, Canada
- **Adeline Rollin** CHU, CNR-MAJ, Labex Distalz, LiCEND Lille, France
- **Pedro Rosa-Neto** Translational Neuroimaging Laboratory, McGill Centre for Studies in Aging, McGill University, Montreal, Québec, Canada
- **Giacomina Rossi** Fondazione IRCCS Istituto Neurologico Carlo Besta, Milano, Italy
- **Martin Rossor** Dementia Research Centre, Department of Neurodegenerative Disease, UCL Institute of Neurology, Queen Square, London, UK
- **Beatriz Santiago** Neurology Department, Centro Hospitalar e Universitario de Coimbra, Coimbra, Portugal
- **Dario Saracino** Sorbonne Université, Paris Brain Institute – Institut du Cerveau – ICM, Inserm U1127, CNRS UMR 7225, AP-HP - Hôpital Pitié-Salpêtrière, Paris, France
- **Sabrina Sayah** Sorbonne Université, Paris Brain Institute – Institut du Cerveau – ICM, Inserm U1127, CNRS UMR 7225, AP-HP - Hôpital Pitié-Salpêtrière, Paris, France
- **Elio Scarpini** Fondazione IRCCS Ca' Granda Ospedale Maggiore Policlinico, Neurodegenerative Diseases Unit, Milan, Italy; University of Milan, Centro Dino Ferrari, Milan, Italy
- **Sonja Schönecker** Neurologische Klinik, Ludwig-Maximilians-Universität München, Munich, Germany
- **Rachelle Shafei** Department of Neurodegenerative Disease, Dementia Research Centre, UCL Institute of Neurology, Queen Square, London, UK
- **Christen Shoesmith** Department of Clinical Neurological Sciences, University of Western Ontario, London, Ontario, Canada
- **Imogen Swift** Department of Neurodegenerative Disease, Dementia Research Centre, UCL Institute of Neurology, Queen Square, London, UK

- **Miguel Tábuas-Pereira** Neurology Department, Centro Hospitalar e Universitario de Coimbra, Coimbra, Portugal
- **Mikel Tainta** Neuroscience Area, Biodonostia Health Research Insitute, San Sebastian, Gipuzkoa, Spain
- **Ricardo Taipa** Neuropathology Unit and Department of Neurology, Centro Hospitalar do Porto - Hospital de Santo António, Oporto, Portugal
- **David Tang-Wai** The University Health Network, Krembil Research Institute, Toronto, Canada
- **David L Thomas** Neuroimaging Analysis Centre, Department of Brain Repair and Rehabilitation, UCL Institute of Neurology, Queen Square, London, UK
- **Paul Thompson** Division of Neuroscience and Experimental Psychology, Wolfson Molecular Imaging Centre, University of Manchester, Manchester, UK
- **Hakan Thonberg** Center for Alzheimer Research, Division of Neurogeriatrics, Karolinska Institutet, Stockholm, Sweden
- **Carolyn Timberlake** Department of Clinical Neurosciences, University of Cambridge, Cambridge, UK
- **Pietro Tiraboschi** Fondazione IRCCS Istituto Neurologico Carlo Besta, Milano, Italy
- **Philip Van Damme** Neurology Service, University Hospitals Leuven, Belgium; Laboratory for Neurobiology, VIB-KU Leuven Centre for Brain Research, Leuven, Belgium
- **Mathieu Vandenbulcke** Geriatric Psychiatry Service, University Hospitals Leuven, Belgium; Neuropsychiatry, Department of Neurosciences, KU Leuven, Leuven, Belgium
- **Michele Veldsman** Nuffield Department of Clinical Neurosciences, Medical Sciences Division, University of Oxford, Oxford, UK
- **Ana Verdelho** Department of Neurosciences and Mental Health, Centro Hospitalar Lisboa Norte - Hospital de Santa Maria & Faculty of Medicine, University of Lisbon, Lisbon, Portugal
- **Jorge Villanua** OSATEK, University of Donostia, San Sebastian, Gipuzkoa, Spain
- **Jason Warren** Department of Neurodegenerative Disease, Dementia Research Centre, UCL Institute of Neurology, Queen Square, London, UK
- **Carlo Wilke** Department of Neurodegenerative Diseases, Hertie-Institute for Clinical Brain Research and Center of Neurology, University of Tübingen, Tübingen, Germany; Center for Neurodegenerative Diseases (DZNE), Tübingen, Germany
- **Ione Woollacott** Department of Neurodegenerative Disease, Dementia Research Centre, UCL Institute of Neurology, Queen Square, London, UK
- **Elisabeth Wlasich** Neurologische Klinik, Ludwig-Maximilians-Universität München, Munich, Germany
- **Henrik Zetterberg** Dementia Research Institute, Department of Neurodegenerative Disease, UCL Institute of Neurology, Queen Square, London, UK
- **Miren Zulaica** Neuroscience Area, Biodonostia Health Research Insitute, San Sebastian, Gipuzkoa, Spain

References

Abrol, A., Damaraju, E., Miller, R.L., Stephen, J.M., Claus, E.D., Mayer, A.R., Calhoun, V.D., 2017. Replicability of time-varying connectivity patterns in large resting state fMRI samples. NeuroImage 163, 160–176. https://doi.org/S1053-8119(17)30768-1 [pii]

Allen, E.A., Damaraju, E., Eichele, T., Wu, L., Calhoun, V.D., 2018. EEG Signatures of Dynamic Functional Network Connectivity States. Brain Topography 31. https://doi.org/10.1007/s10548-017-0546-2

Allen, E.A., Damaraju, E., Plis, S.M., Erhardt, E.B., Eichele, T., Calhoun, V.D., 2014. Tracking whole-brain connectivity dynamics in the resting state. Cerebral cortex (New York, N.Y.: 1991) 24, 663–676. https://doi.org/10.1093/cercor/bhs352 [doi]

Allen, E.A., Erhardt, E.B., Damaraju, E., Gruner, W., Segall, J.M., Silva, R.F., Havlicek, M., Rachakonda, S., Fries, J., Kalyanam, R., Michael, A.M., Caprihan, A., Turner, J.A., Eichele, T., Adelsheim, S., Bryan, A.D., Bustillo, J., Clark, V.P., Ewing, S.W.F., Filbey, F., Ford, C.C., Hutchison, K., Jung, R.E., Kiehl, K.A., Kodituwakku, P., Komesu, Y.M., Mayer, A.R., Pearlson, G.D., Phillips, J.P., Sadek, J.R., Stevens, M., Teuscher, U., Thoma, R.J., Calhoun, V.D., 2011. A baseline for the multivariate comparison of resting-state networks. Frontiers in systems neuroscience 5, 2. https://doi.org/10.3389/fnsys.2011.00002 [doi]

Arthur, D., Vassilvitskii, S., 2007. k-means++: the advantages of careful seeding., in: SODA '07. Society for Industrial and Applied Mathematics, pp. 1027–1035.

Baker, M., Mackenzie, I.R., Pickering-Brown, S.M., Gass, J., Rademakers, R., Lindholm, C., Snowden, J., Adamson, J., Sadovnick, A.D., Rollinson, S., Cannon, A., Dwosh, E., Neary, D., Melquist, S., Richardson, A., Dickson, D., Berger, Z., Eriksen, J., Robinson, T., Zehr, C., Dickey, C.A., Crook, R., McGowan, E., Mann, D., Boeve, B., Feldman, H., Hutton, M., 2006. Mutations in progranulin cause tau-negative frontotemporal dementia linked to chromosome 17. Nature 442, 916–919. https://doi.org/10.1038/nature05016

Benjamini, Y., Hochberg, Y., 1995. Controlling the False Discovery Rate: A Practical and Powerful Approach to Multiple Testing. Journal of the Royal Statistical Society. Series B, Methodological 57, 289–300. https://doi.org/10.1111/j.2517-6161.1995.tb02031.x

Borrego-Écija, S., Sala-Llonch, R., van Swieten, J., Borroni, B., Moreno, F., Masellis, M., Tartaglia, C., Graff, C., Galimberti, D., Jr, R.L., Rowe, J.B., Finger, E., Vandenberghe, R., Tagliavini, F., de Mendonça, A., Santana, I., Synofzik, M., Ducharme, S., Levin, J., Danek, A., Gerhard, A., Otto, M., Butler, C., Frisoni, G., Sorbi, S., Heller, C., Bocchetta, M., Cash, D.M., Convery, R.S., Moore, K.M., Rohrer, J.D., Sanchez-Valle, R., GENFI, G.F.T.D.I., 2021. Disease-related cortical thinning in presymptomatic granulin mutation carriers. NeuroImage.Clinical 29, 102540. https://doi.org/S2213-1582(20)30377-6 [pii]

Borroni, B., Alberici, A., Cercignani, M., Premi, E., Serra, L., Cerini, C., Cosseddu, M., Pettenati, C., Turla, M., Archetti, S., Gasparotti, R., Caltagirone, C., Padovani, A., Bozzali, M., 2012. Granulin mutation drives brain damage and reorganization from preclinical to symptomatic FTLD. Neurobiology of Aging 33, 2506–2520. https://doi.org/10.1016/j.neurobiolaging.2011.10.031

Bowie, C.R., Harvey, P.D., 2006. Administration and interpretation of the Trail Making Test. Nature protocols 1, 2277–2281. https://doi.org/nprot.2006.390 [pii]

Calhoun, V.D., Miller, R., Pearlson, G., Adalı, T., 2014. The chronnectome: time-varying connectivity networks as the next frontier in fMRI data discovery. Neuron 84, 262–274. https://doi.org/S0896-6273(14)00913-1 [pii]

Calhoun, V.D., Wager, T.D., Krishnan, A., Rosch, K.S., Seymour, K.E., Nebel, M.B., Mostofsky, S.H., Nyalakanai, P., Kiehl, K., 2017. The impact of T1 versus EPI spatial normalization templates for fMRI data analyses. Human brain mapping 38, 5331–5342. https://doi.org/10.1002/hbm.23737 [doi]

Cash, D.M., Bocchetta, M., Thomas, D.L., Dick, K.M., van Swieten, J.C., Borroni, B., Galimberti, D., Masellis, M., Tartaglia, M.C., Rowe, J.B., Graff, C., Tagliavini, F., Frisoni, G.B., Jr, R.L., Finger, E., de Mendonça, A., Sorbi, S., Rossor, M.N., Ourselin, S., Rohrer, J.D., Initiative, G.G.F.T.D., 2018. Patterns of gray matter atrophy in genetic frontotemporal dementia: results from the GENFI study. Neurobiology of aging 62, 191–196. https://doi.org/S0197-4580(17)30347-0 [pii]

Chitramuthu, B.P., Bennett, H.P.J., Bateman, A., 2017. Progranulin: a new avenue towards the understanding and treatment of neurodegenerative disease. Brain : a journal of neurology 140, 3081–3104. https://doi.org/10.1093/brain/awx198 [doi]

Cruts, M., Gijselinck, I., van der Zee, J., Engelborghs, S., Wils, H., Pirici, D., Rademakers, R., Vandenberghe, R., Dermaut, B., Martin, J.-J., van Duijn, C., Peeters, K., Sciot, R., Santens, P., De Pooter, T., Mattheijssens, M., Van den Broeck, M., Cuijt, I., Vennekens, K., De Deyn, P.P., Kumar-Singh, S., Van Broeckhoven, C., 2006. Null mutations in progranulin cause ubiquitin-positive frontotemporal dementia linked to chromosome 17q21. Nature 442, 920–4. https://doi.org/10.1038/nature05017

Damaraju, E., Tagliazucchi, E., Laufs, H., Calhoun, V.D., 2020. Connectivity dynamics from wakefulness to sleep. NeuroImage 220. https://doi.org/10.1016/j.neuroimage.2020.117047

Dopper, E.G., Rombouts, S.A., Jiskoot, L.C., Heijer, T., de Graaf, J.R., Koning, I., Hammerschlag, A.R., Seelaar, H., Seeley, W.W., Veer, I.M., van Buchem, M.A., Rizzu, P., van Swieten, J.C., 2013. Structural and functional brain connectivity in presymptomatic familial frontotemporal dementia. Neurology 80, 814–823. https://doi.org/10.1212/WNL.0b013e31828407bc [doi]

Du, Y., Fan, Y., 2013. Group information guided ICA for fMRI data analysis. NeuroImage 69, 157–197. https://doi.org/S1053-8119(12)01104-4 [pii]

Du, Y., Pearlson, G.D., Liu, J., Sui, J., Yu, Q., He, H., Castro, E., Calhoun, V.D., 2015. A group ICA based framework for evaluating resting fMRI markers when disease categories are unclear: application to schizophrenia, bipolar, and schizoaffective disorders. NeuroImage 122, 272–280. https://doi.org/S1053-8119(15)00674-6 [pii]

Feis, R.A., Bouts, M.J.R.J., de Vos, F., Schouten, T.M., Panman, J.L., Jiskoot, L.C., Dopper, E.G.P., van der Grond, J., van Swieten, J.C., Rombouts, S.A.R.B., 2019. A multimodal MRI-based classification signature emerges just prior to symptom onset in frontotemporal dementia mutation carriers. Journal of neurology, neurosurgery, and psychiatry 90, 1207–1214. https://doi.org/10.1136/jnnp-2019-320774 [doi]

Fox, M.D., Snyder, A.Z., Vincent, J.L., Corbetta, M., Essen, D.C. Van, Raichle, M.E., 2005. The human brain is intrinsically organized into dynamic, anticorrelated functional networks. Proceedings of the National Academy of Sciences of the United States of America 102, 9673–9678. https://doi.org/0504136102 [pii]

Gass, J., Cannon, A., Mackenzie, I.R., Boeve, B., Baker, M., Adamson, J., Crook, R., Melquist, S., Kuntz, K., Petersen, R., Josephs, K., Pickering-Brown, S.M., Graff-Radford, N., Uitti, R., Dickson, D., Wszolek, Z., Gonzalez, J., Beach, T.G., Bigio, E., Johnson, N., Weintraub, S., Mesulam, M., 3rd, C.L.W., Woodruff, B., Caselli, R., Hsiung, G.Y., Feldman, H., Knopman, D., Hutton, M., Rademakers, R., 2006. Mutations in progranulin are a major cause of ubiquitin-positive frontotemporal lobar degeneration. Human molecular genetics 15, 2988–3001. https://doi.org/l241 [pii]

Gorno-Tempini, M.L., Hillis, A.E., Weintraub, S., Kertesz, A., Mendez, M., Cappa, S.F., Ogar, J.M., Rohrer, J.D., Black, S., Boeve, B.F., Manes, F., Dronkers, N.F., Vandenberghe, R., Rascovsky, K., Patterson, K., Miller, B.L., Knopman, D.S., Hodges, J.R., Mesulam, M.M., Grossman, M., 2011. Classification of primary progressive aphasia and its variants. Neurology 76, 1006–1014. https://doi.org/10.1212/WNL.0b013e31821103e6

Iraji, A., Deramus, T.P., Lewis, N., Yaesoubi, M., Stephen, J.M., Erhardt, E., Belger, A., Ford, J.M., McEwen, S., Mathalon, D.H., Mueller, B.A., Pearlson, G.D., Potkin, S.G., Preda, A., Turner, J.A., Vaidya, J.G., van Erp, T.G.M., Calhoun, V.D., 2019a. The spatial chronnectome

reveals a dynamic interplay between functional segregation and integration. Human brain mapping 40, 3058–3077. https://doi.org/10.1002/hbm.24580 [doi]
Iraji, Armin, Faghiri, A., Lewis, N., Fu, Z., Rachakonda, S., Calhoun, V.D., 2020. Tools of the trade: Estimating time-varying connectivity patterns from fMRI data. Social cognitive and affective neuroscience. https://doi.org/10.1093/scan/nsaa114
Iraji, A., Fu, Z., Damaraju, E., DeRamus, T.P., Lewis, N., Bustillo, J.R., Lenroot, R.K., Belger, A., Ford, J.M., McEwen, S., Mathalon, D.H., Mueller, B.A., Pearlson, G.D., Potkin, S.G., Preda, A., Turner, J.A., Vaidya, J.G., van Erp, T.G.M., Calhoun, V.D., 2019b. Spatial dynamics within and between brain functional domains: A hierarchical approach to study time-varying brain function. Human brain mapping 40, 1969–1986. https://doi.org/10.1002/hbm.24505 [doi]
Iraji, A, Miller, R., Adali, T., Calhoun, V.D., 2020. Space: A Missing Piece of the Dynamic Puzzle. Trends in cognitive sciences 24, 135–149. https://doi.org/S1364-6613(19)30292-X [pii]
Lee, S.E., Sias, A.C., Kosik, E.L., Flagan, T.M., Deng, J., Chu, S.A., Brown, J.A., Vidovszky, A.A., Ramos, E.M., Gorno-Tempini, M.L., Karydas, A.M., Coppola, G., Geschwind, D.H., Rademakers, R., Boeve, B.F., Boxer, A.L., Rosen, H.J., Miller, B.L., Seeley, W.W., 2019. Thalamo-cortical network hyperconnectivity in preclinical progranulin mutation carriers. NeuroImage.Clinical 22, 101751. https://doi.org/S2213-1582(19)30101-9 [pii]
Lurie, D.J., Kessler, D., Bassett, D.S., Betzel, R.F., Breakspear, M., Kheilholz, S., Kucyi, A., Liégeois, R., Lindquist, M.A., McIntosh, A.R., Poldrack, R.A., Shine, J.M., Thompson, W.H., Bielczyk, N.Z., Douw, L., Kraft, D., Miller, R.L., Muthuraman, M., Pasquini, L., Razi, A., Vidaurre, D., Xie, H., Calhoun, V.D., 2020. Questions and controversies in the study of time-varying functional connectivity in resting fMRI. Network neuroscience (Cambridge, Mass.) 4, 30–69. https://doi.org/10.1162/netn_a_00116
Miller, R.L., Yaesoubi, M., Turner, J.A., Mathalon, D., Preda, A., Pearlson, G., Adali, T., Calhoun, V.D., 2016. Higher Dimensional Meta-State Analysis Reveals Reduced Resting fMRI Connectivity Dynamism in Schizophrenia Patients. PloS one 11, e0149849. https://doi.org/10.1371/journal.pone.0149849 [doi]
Moore, K.M., Nicholas, J., Grossman, M., McMillan, C.T., Irwin, D.J., Massimo, L., Van Deerlin, V.M., Warren, J.D., Fox, N.C., Rossor, M.N., Mead, S., Bocchetta, M., Boeve, B.F., Knopman, D.S., Graff-Radford, N.R., Forsberg, L.K., Rademakers, R., Wszolek, Z.K., van Swieten, J.C., Jiskoot, L.C., Meeter, L.H., Dopper, E.G., Papma, J.M., Snowden, J.S., Saxon, J., Jones, M., Pickering-Brown, S., Le Ber, I., Camuzat, A., Brice, A., Caroppo, P., Ghidoni, R., Pievani, M., Benussi, L., Binetti, G., Dickerson, B.C., Lucente, D., Krivensky, S., Graff, C., Öijerstedt, L., Fallström, M., Thonberg, H., Ghoshal, N., Morris, J.C., Borroni, B., Benussi, A., Padovani, A., Galimberti, D., Scarpini, E., Fumagalli, G.G., Mackenzie, I.R., Hsiung, G.Y.R., Sengdy, P., Boxer, A.L., Rosen, H., Taylor, J.B., Synofzik, M., Wilke, C., Sulzer, P., Hodges, J.R., Halliday, G., Kwok, J., Sanchez-Valle, R., Lladó, A., Borrego-Ecija, S., Santana, I., Almeida, M.R., Tábuas-Pereira, M., Moreno, F., Barandiaran, M., Indakoetxea, B., Levin, J., Danek, A., Rowe, J.B., Cope, T.E., Otto, M., Anderl-Straub, S., de Mendonça, A., Maruta, C., Masellis, M., Black, S.E., Couratier, P., Lautrette, G., Huey, E.D., Sorbi, S., Nacmias, B., Laforce, R., Tremblay, M.P.L., Vandenberghe, R., Damme, P. Van, Rogalski, E.J., Weintraub, S., Gerhard, A., Onyike, C.U., Ducharme, S., Papageorgiou, S.G., Ng, A.S.L., Brodtmann, A., Finger, E., Guerreiro, R., Bras, J., Rohrer, J.D., Heller, C., Convery, R.S., Woollacott, I.O., Shafei, R.M., Graff-Radford, J., Jones, D.T., Dheel, C.M., Savica, R., Lapid, M.I., Baker, M., Fields, J.A., Gavrilova, R., Domoto-Reilly, K., Poos, J.M., Van der Ende, E.L., Panman, J.L., Donker Kaat, L., Seelaar, H., Richardson, A., Frisoni, G., Mega, A., Fostinelli, S., Chiang, H.H., Alberici, A., Arighi, A., Fenoglio, C., Heuer, H., Miller, B., Karydas, A., Fong, J., João Leitão, M., Santiago, B., Duro, D., Ferreira, Carlos, Gabilondo, A., De Arriba, M., Tainta, M., Zulaica, M., Ferreira, Catarina, Semler, E., Ludolph, A., Landwehrmeyer, B., Volk, A.E., Miltenberger, G., Verdelho, A., Afonso, S., Tartaglia, M.C., Freedman, M., Rogaeva, E., Ferrari, C., Piaceri, I., Bessi, V., Lombardi, G., St-Onge, F., Doré, M.C., Bruffaerts, R.,

Vandenbulcke, M., Van den Stock, J., Mesulam, M.M., Bigio, E., Koros, C., Papatriantafyllou, J., Kroupis, C., Stefanis, L., Shoesmith, C., Robertson, E., Coppola, G., Da Silva Ramos, E.M., Geschwind, D., 2020. Age at symptom onset and death and disease duration in genetic frontotemporal dementia: an international retrospective cohort study. The Lancet Neurology 19, 145–156. https://doi.org/10.1016/S1474-4422(19)30394-1

Panman, J.L., Venkatraghavan, V., van der Ende, E.L., Steketee, R.M.E., Jiskoot, L.C., Poos, J.M., Dopper, E.G.P., Meeter, L.H.H., Kaat, L.D., Rombouts, S.A.R.B., Vernooij, M.W., Kievit, A.J.A., Premi, E., Cosseddu, M., Bonomi, E., Olives, J., Rohrer, J.D., Sánchez-Valle, R., Borroni, B., Bron, E.E., Swieten, J.C. Van, Papma, J.M., Klein, S., consortium investigators, G., 2021. Modelling the cascade of biomarker changes in GRN-related frontotemporal dementia. Journal of neurology, neurosurgery, and psychiatry. https://doi.org/jnnp-2020-323541 [pii]

Power, J.D., Barnes, K.A., Snyder, A.Z., Schlaggar, B.L., Petersen, S.E., 2012. Spurious but systematic correlations in functional connectivity MRI networks arise from subject motion. NeuroImage 59, 2142–2154. https://doi.org/10.1016/j.neuroimage.2011.10.018 [doi]

Premi, E., Calhoun, V.D., Diano, M., Gazzina, S., Cosseddu, M., Alberici, A., Archetti, S., Paternicò, D., Gasparotti, R., van Swieten, J., Galimberti, D., Sanchez-Valle, R., Laforce, R., Moreno, F., Synofzik, M., Graff, C., Masellis, M., Tartaglia, M.C., Rowe, J., Vandenberghe, R., Finger, E., Tagliavini, F., de Mendonça, A., Santana, I., Butler, C., Ducharme, S., Gerhard, A., Danek, A., Levin, J., Otto, M., Frisoni, G., Cappa, S., Sorbi, S., Padovani, A., Rohrer, J.D., Borroni, B., 2019. The inner fluctuations of the brain in presymptomatic Frontotemporal Dementia: The chronnectome fingerprint. NeuroImage 189. https://doi.org/10.1016/j.neuroimage.2019.01.080

Premi, E., Cauda, F., Costa, T., Diano, M., Gazzina, S., Gualeni, V., Alberici, A., Archetti, S., Magoni, M., Gasparotti, R., Padovani, A., Borroni, B., 2016. Looking for Neuroimaging Markers in Frontotemporal Lobar Degeneration Clinical Trials: A Multi-Voxel Pattern Analysis Study in Granulin Disease. Journal of Alzheimer's Disease 51. https://doi.org/10.3233/JAD-150340

Premi, Enrico, Cauda, F., Gasparotti, R., Diano, M., Archetti, S., Padovani, A., Borroni, B., 2014. Multimodal FMRI resting-state functional connectivity in granulin mutations: the case of fronto-parietal dementia. PloS one 9, e106500. https://doi.org/10.1371/journal.pone.0106500

Premi, E., Formenti, A., Gazzina, S., Archetti, S., Gasparotti, R., Padovani, A., Borroni, B., 2014. Effect of TMEM106B polymorphism on functional network connectivity in asymptomatic GRN mutation carriers. JAMA Neurology 71. https://doi.org/10.1001/jamaneurol.2013.4835

Rascovsky, K., Hodges, J.R., Knopman, D., Mendez, M.F., Kramer, J.H., Neuhaus, J., Van Swieten, J.C., Seelaar, H., Dopper, E.G.P., Onyike, C.U., Hillis, A.E., Josephs, K.A., Boeve, B.F., Kertesz, A., Seeley, W.W., Rankin, K.P., Johnson, J.K., Gorno-Tempini, M.L., Rosen, H., Prioleau-Latham, C.E., Lee, A., Kipps, C.M., Lillo, P., Piguet, O., Rohrer, J.D., Rossor, M.N., Warren, J.D., Fox, N.C., Galasko, D., Salmon, D.P., Black, S.E., Mesulam, M., Weintraub, S., Dickerson, B.C., Diehl-Schmid, J., Pasquier, F., Deramecourt, V., Lebert, F., Pijnenburg, Y., Chow, T.W., Manes, F., Grafman, J., Cappa, S.F., Freedman, M., Grossman, M., Miller, B.L., 2011. Sensitivity of revised diagnostic criteria for the behavioural variant of frontotemporal dementia. Brain 134, 2456–2477. https://doi.org/10.1093/brain/awr179

Raut, R. v., Snyder, A.Z., Mitra, A., Yellin, D., Fujii, N., Malach, R., Raichle, M.E., 2021. Global waves synchronize the brain's functional systems with fluctuating arousal. Science Advances 7. https://doi.org/10.1126/sciadv.abf2709

Rohrer, J.D., Nicholas, J.M., Cash, D.M., van Swieten, J., Dopper, E., Jiskoot, L., van Minkelen, R., Rombouts, S.A., Cardoso, M.J., Clegg, S., Espak, M., Mead, S., Thomas, D.L., De Vita, E., Masellis, M., Black, S.E., Freedman, M., Keren, R., MacIntosh, B.J., Rogaeva, E., Tang-Wai, D., Tartaglia, M.C., Laforce, R., Tagliavini, F., Tiraboschi, P., Redaelli, V., Prioni, S., Grisoli, M., Borroni, B., Padovani, A., Galimberti, D., Scarpini, E., Arighi, A., Fumagalli, G., Rowe,

J.B., Coyle-Gilchrist, I., Graff, C., Fallström, M., Jelic, V., Ståhlbom, A.K., Andersson, C., Thonberg, H., Lilius, L., Frisoni, G.B., Pievani, M., Bocchetta, M., Benussi, L., Ghidoni, R., Finger, E., Sorbi, S., Nacmias, B., Lombardi, G., Polito, C., Warren, J.D., Ourselin, S., Fox, N.C., Rossor, M.N., 2015. Presymptomatic cognitive and neuroanatomical changes in genetic frontotemporal dementia in the Genetic Frontotemporal dementia Initiative (GENFI) study: A cross-sectional analysis. The Lancet Neurology 14, 253–262. https://doi.org/10.1016/S1474-4422(14)70324-2

Saha, D.K., Damaraju, E., Rashid, B., Abrol, A., Plis, S.M., Calhoun, V.D., 2021. A Classification-Based Approach to Estimate the Number of Resting Functional Magnetic Resonance Imaging Dynamic Functional Connectivity States. Brain connectivity. https://doi.org/10.1089/brain.2020.0794 [doi]

Salman, M.S., Du, Y., Lin, D., Fu, Z., Fedorov, A., Damaraju, E., Sui, J., Chen, J., Mayer, A.R., Posse, S., Mathalon, D.H., Ford, J.M., Van Erp, T., Calhoun, V.D., 2019. Group ICA for identifying biomarkers in schizophrenia: "Adaptive" networks via spatially constrained ICA show more sensitivity to group differences than spatio-temporal regression. NeuroImage. Clinical 22, 101747. https://doi.org/10.1016/j.nicl.2019.101747

Seeley, W.W., Menon, V., Schatzberg, A.F., Keller, J., Glover, G.H., Kenna, H., Reiss, A.L., Greicius, M.D., 2007. Dissociable intrinsic connectivity networks for salience processing and executive control. The Journal of neuroscience : the official journal of the Society for Neuroscience 27, 2349–2356. https://doi.org/27/9/2349 [pii]

Tagliazucchi, E., Laufs, H., 2014. Decoding wakefulness levels from typical fMRI resting-state data reveals reliable drifts between wakefulness and sleep. Neuron 82, 695–708. https://doi.org/10.1016/j.neuron.2014.03.020

Tognoli, E., Kelso, J.A., 2014. The metastable brain. Neuron 81, 35–48. https://doi.org/S0896-6273(13)01183-5 [pii]

Uddin, L.Q., Kelly, A.M., Biswal, B.B., Castellanos, F.X., Milham, M.P., 2009. Functional connectivity of default mode network components: correlation, anticorrelation, and causality. Human brain mapping 30, 625–637. https://doi.org/10.1002/hbm.20531 [doi]

Wang, J., Han, J., Nguyen, V.T., Guo, L., Guo, C.C., 2017. Improving the Test-Retest Reliability of Resting State fMRI by Removing the Impact of Sleep. Frontiers in neuroscience 11, 249. https://doi.org/10.3389/fnins.2017.00249

White, T., Calhoun, V.D., 2019. Dissecting Static and Dynamic Functional Connectivity: Example From the Autism Spectrum. Journal of experimental neuroscience 13, 1179069519851809. https://doi.org/10.1177/1179069519851809 [doi]

Yan, C.G., Wang, X.D., Zuo, X.N., Zang, Y.F., 2016. DPABI: Data Processing & Analysis for (Resting-State) Brain Imaging. Neuroinformatics 14, 339–351. https://doi.org/10.1007/s12021-016-9299-4 [doi]

Zhou, J., Greicius, M.D., Gennatas, E.D., Growdon, M.E., Jang, J.Y., Rabinovici, G.D., Kramer, J.H., Weiner, M., Miller, B.L., Seeley, W.W., 2010. Divergent network connectivity changes in behavioural variant frontotemporal dementia and Alzheimer ' s disease 1352–1367. https://doi.org/10.1093/brain/awq075

Table 1. Demographic characteristics of included subjects.

Variable	HC N=282	*GRN* N=141	P-value*
Age (years)	46.5±13.2	45.9±11.9	0.650
Female, % (number)	57.4 (162)	63.8 (90)	0.207^
Education (years)	14.3±3.3	14.6±3.5	0.395
Years from expected onset (years)	-	-14.1±12.1	-
Framewise displacement (FD)	0.16±0.1	0.17±0.1	0.246
Insular volume (% of TIV)	0.76±0.07	0.76±0.07	0.540
Cognitive assessment			
Boston Naming test (score)	27.9±2.1	27.9±2.0	0.976°
TMT, part A (sec)	27.7±12.5	28.5±10.1	0.318°
TMT, part B (sec)	66.7±33.7	65.9±31.2	0.882°

*Student t-test unless otherwise specified; ^Chi-Square test; °univariate General Linear Model corrected for age and gender.

Results are expressed as mean ± standard deviation, otherwise specified. HC = Healthy Controls; *GRN* = Granulin; TMT = Trial Making Test; TIV = total intracranial volume

Table 2. Mean dwell time (in each spatial state according to considered dynamic functional networks) in HC and in presymptomatic mutation carriers.

Large-scale networks	HC N=282	*GRN* N=141
Default Mode Network		
Spatial State 1	16.0±1.0	15.6±1.6
Spatial State 2	22.3±1.5	**28.3±2.9***
Spatial State 3	10.1±1.2	10.0±1.4
Spatial State 4	18.4±1.3	15.8±2.0
Language Network		
Spatial State 1	16.4±1.1	14.2±1.5
Spatial State 2	25.2±1.5	20.5±2.1
Spatial State 3	9.4±1.1	10.3±1.8
Spatial State 4	15.5±1.1	**25.0±2.6***
Salience Network		
Spatial State 1	12.3±0.9	**16.3±1.7***
Spatial State 2	12.2±0.9	12.7±1.5
Spatial State 3	18.8±1.1	19.3±1.8
Spatial State 4	21.1±1.3	**15.1±1.6***

Mean dwell time results are reported as mean ± standard error. Dwell time is expressed in seconds. HC = Healthy Controls; *GRN* = Granulin; TIV= total intracranial volume.

*significant p-values<0.05, False Discovery Rate (FDR)-corrected as compared to HC (corrected for age, gender, site, framewise displacement-FD and insular volume (as % of TIV)).

Legend to figures

Figure 1. Spatial states of the default mode network (DMN) and mean dwell time differences between presymptomatic *GRN* mutation carriers and healthy controls.

The spatial states of the default mode network. Hot and cold colours represent positive and negative associations to the default mode, respectively. Significant dwell-time differences between groups were reported ($p<0.05$ FDR-corrected). Maps of each spatial states are displayed on a standardized axial T1 MRI template, z-axis coordinates are reported under each slice.

DMN = default mode network; *GRN* = presymptomatic *granulin* mutation carriers; HC = healthy controls.

Figure 2. Spatial states of the language network (LN) and mean dwell time differences between presymptomatic *GRN* mutation carriers and healthy controls.

The spatial states of the language network. Hot and cold colours represent positive and negative associations to the language network, respectively. Significant dwell-time differences between groups were reported ($p<0.05$ FDR-corrected). Maps of each spatial states are displayed on a standardized axial T1 MRI template, z-axis coordinates are reported under each slice.

LN = Language Network; *GRN* = presymptomatic *granulin* mutation carriers; HC = healthy controls.

Figure 3. Spatial states of the salience network (SN) and mean dwell time differences between presymptomatic *GRN* mutation carriers and healthy controls.

The spatial states of the salience network. Hot and cold colours represent positive and negative associations to the salience network, respectively. Significant dwell-time differences between

groups were reported ($p<0.05$ FDR-corrected). Maps of each spatial states are displayed on a standardized axial T1 MRI template, z-axis coordinates are reported under each slice.

SN = salience network; *GRN* = presymptomatic *granulin* mutation carriers; HC = healthy controls.

Figure 1.

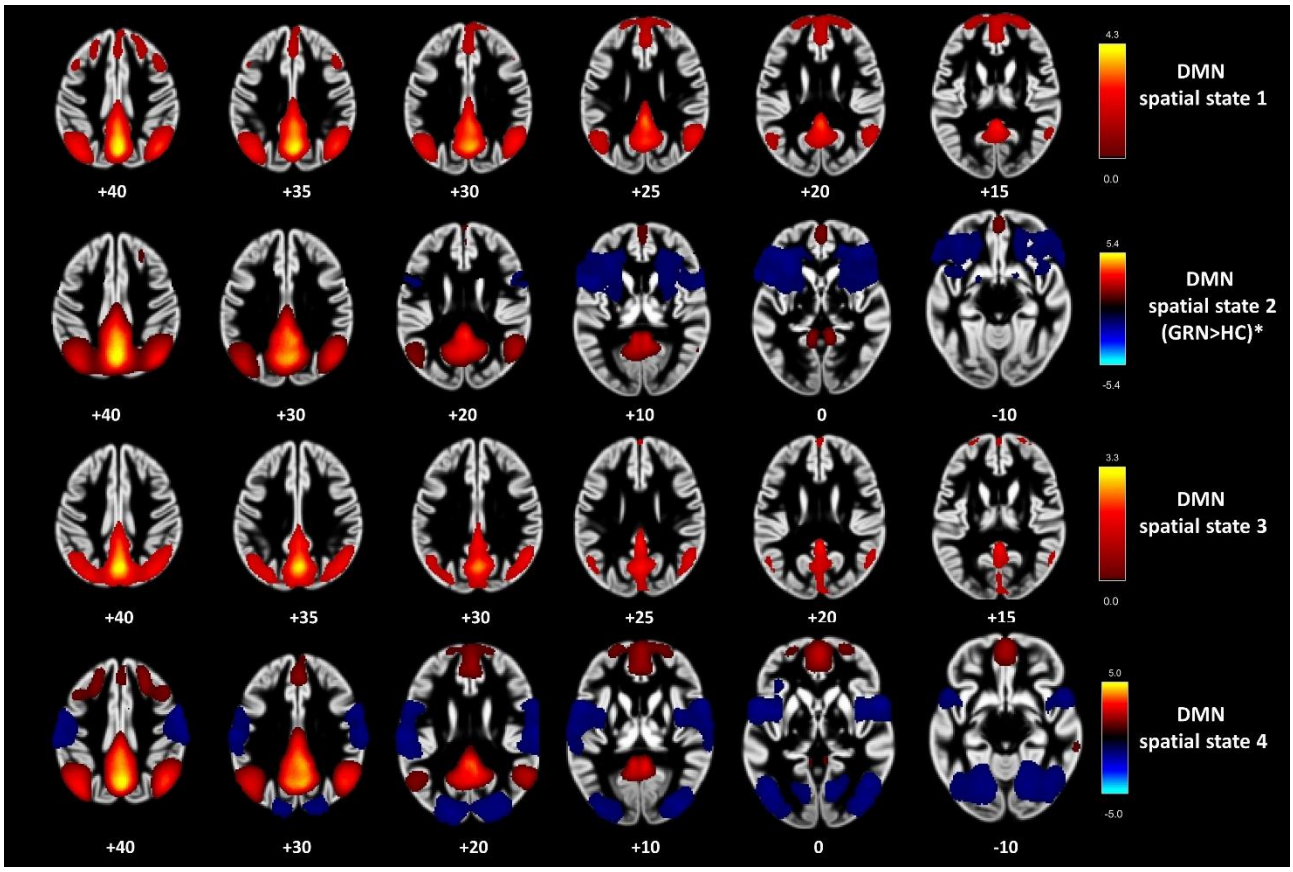
+40
+35
+30
+25
+20
+15
4.3
0.0
DMN
spatial state 1
+40
+30
+20
+10
0
-10
5.4
-5.4
DMN
spatial state 2
(GRN>HC)*
+40
+35
+30
+25
+20
+15
3.3
0.0
DMN
spatial state 3
+40
+30
+20
+10
0
-10
5.0
-5.0
DMN
spatial state 4

Figure 2.

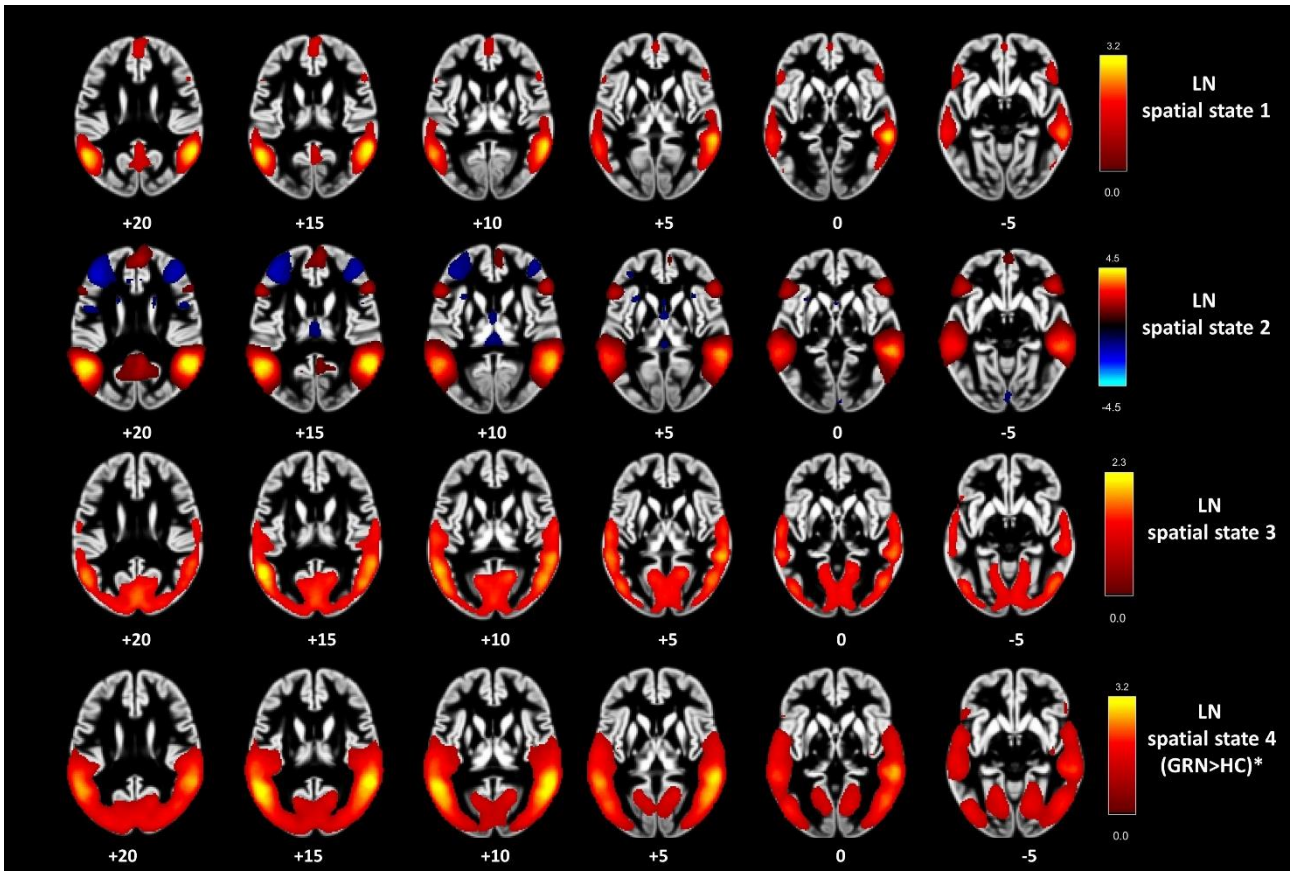
+20
+15
+10
+5
0
-5
3.2
0.0
LN
spatial state 1
4.5
-4.5
LN
spatial state 2
2.3
LN
spatial state 3
LN
spatial state 4
(GRN>HC)*

Figure 3.

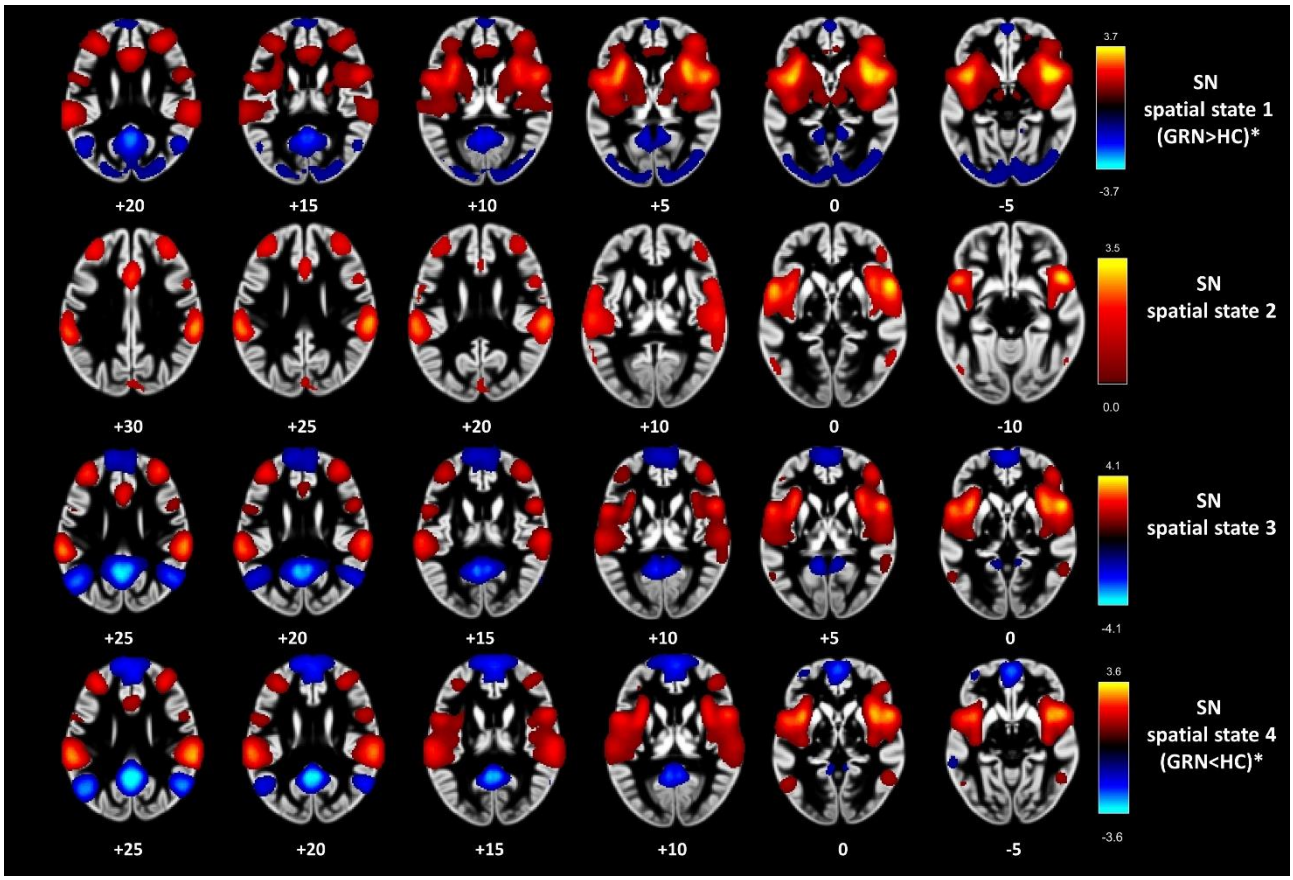
+20
+15
+10
+5
0
-5
3.7
-3.7
SN
spatial state 1
(GRN>HC)*
+30
+25
+20
+10
0
-10
3.5
0.0
SN
spatial state 2
+25
+20
+15
+10
+5
0
4.1
-4.1
SN
spatial state 3
+25
+20
+15
+10
0
-5
3.6
-3.6
SN
spatial state 4
(GRN<HC)*

Supplementary Table 1. Detailed MRI acquisition parameters of all included GENFI centers.

centre	subjects (n)	Scanner	TR	TE	volumes	volume slices	slice thickness	slice gap	pixel spacing	FOV	slice order
1	17	Siemens Trio	2200	30	140	36	3.3	3.3	3.3125\3.3125	58*64	interleaved
2	28	Philips Achieva	2200	30	140	36	3.3	3.3	2.650\2.650	63*64	interleaved
3	89	Philips Achieva	2200	30	200	38	2.7	3.0	2.75\2.75	80*80	interleaved
4	3	Philips Achieva	2500	30	200	42	3.5	3.5	3\3	64*64	interleaved
5	29	Siemens Prisma	2500	30	200	42	3.3	3.3	3.4375\3.4375	64*64	interleaved
6	9	Philips Achieva	2500	30	200	42	3.5	3.5	3\3	64*64	interleaved
7	12	Siemens Prisma	2500	30	200	42	3.5	3.5	3\3	64*64	interleaved
8	41	Siemens Skyra	2500	30	200	42	3.5	3.5	3\3	64*64	interleaved
9	22	Siemens Trio	2500	30	200	42	3.5	3.5	3\3	64*64	interleaved
10	26	Siemens Skyra	2500	30	200	42	3.5	3.5	3\3	64*64	interleaved
11	25	Siemens Prisma	2500	30	200	42	3.5	3.5	3\3	64*64	interleaved
12	9	Siemens Trio	2500	30	200	42	3.5	3.5	3\3	64*64	interleaved
13	37	Philips Achieva	2500	30	200	42	3.5	3.5	3\3	64*64	interleaved
14	16	Siemens Trio	2500	30	200	42	3.5	3.5	3\3	64*64	interleaved
15	9	Siemens Trio	2200	30	140	36	3.3	3.3	3.3125\3.3125	58*64	interleaved
16	13	Siemens Trio	2500	30	200	42	3.5	3.5	3\3	64*64	interleaved
17	26	Siemens Trio	2500	30	200	42	3.5	3.5	3\3	64*64	interleaved
18	1	Philips Achieva	2500	30	200	42	3.5	3.5	3\3	64*64	interleaved
19	9	Siemens Prisma	2500	30	200	42	3.5	3.5	3\3	64*64	interleaved
20	1	Siemens Prisma	2500	30	200	42	3.5	3.5	3\3	64*64	interleaved
21	1	GE Signa	2500	30	200	36	3.5	3.5	3\3	64*64	interleaved

TR: repetition time; TE: echo time, FOV: field of view, GE: General Electric, n: number.

Supplementary Table 2. Mean fractional occupancy (FO) (in each spatial state according to considered dynamic functional networks) and total number of transitions (TN) in HC and in presymptomatic mutation carriers.

Large-scale networks	HC N=282	*GRN* N=141
Default Mode Network		
Spatial State 1	0.27±0.25	0.26±0.26
Spatial State 2	0.34±0.30	0.38±0.35
Spatial State 3	0.13±0.24	0.15±0.26
Spatial State 4	**0.27±0.26**	**0.21±0.24***
Total number of transitions	3.9±2.2	3.7±2.5
Language Network		
Spatial State 1	0.26±0.25	0.22±0.22
Spatial State 2	**0.37±0.30**	**0.30±0.29***
Spatial State 3	0.12±0.22	0.13±0.25
Spatial State 4	**0.26±0.25**	**0.35±0.32***
Transition number	4.0±2.3	3.8±2.4
Salience Network		
Spatial State 1	**0.18±0.22**	**0.24±0.26***
Spatial State 2	0.17±0.21	0.17±0.23
Spatial State 3	0.36±0.24	0.35±0.25
Spatial State 4	**0.30±0.28**	**0.24±0.27***
Transition number	4.5±2.1	4.7±2.3

Mean fractional occupancy results are reported as mean ± standard error. HC = Healthy Controls; *GRN* = Granulin.

*significant p-values<0.05, False Discovery Rate (FDR)-corrected as compared to HC (corrected for age, gender, site, framewise displacement-FD and insular volume (as % of total intracranial volume)).

Supplementary Figure 1.

Box plots for the significant (p=0.05 FDR-corrected) comparisons (DT and FO) between presymptomatic *GRN* carriers and healthy controls in the selected states of the studied networks. First line: dwell time (DT), second line: fractional occupancy (FO). Box plots with bee swarm representation are reported. Tukey method was used to define the extent of the whiskers, considering the data points that are less than 1.5 x interquartile range away from 1st/3rd quartile. GRN: presymptomatic *GRN* carriers; HC: healthy controls.

Supplementary Figure 2.

Scatterplots of DTs values in presymptomatic *GRN* carriers considering the significant comparisons with HC (DMN state 2, LN state 4, SN state 1 and SN state 4). DT values are reported on both axes. DMN: default mode network; LN: language network; SN: salience network.

Supplementary Figure 3.

Panel A. Static large-scale network maps (DMN, LN and SN) obtained from GIG-ICA.
DMN: Default Mode Network; LN: Language Network; SN: Salience Network; GIG-ICA: Group Information Guided independent component analysis. Most representative axial slices of the 3 spatial maps are plotted as z-score and thresholded at Z >1.5 on an MRI grey matter standardized template; standardized z-axis coordinates are reported.

Panel B: brain connectome showing the selected large-scale networks relationship in the whole group of subjects (both HC and presymptomatic GRN carriers). The colormap represents the magnitude (T value) and the direction (blue: negative correlation, red: positive correlation) of the between-network static functional connectivity.

Supplementary Figure 1.

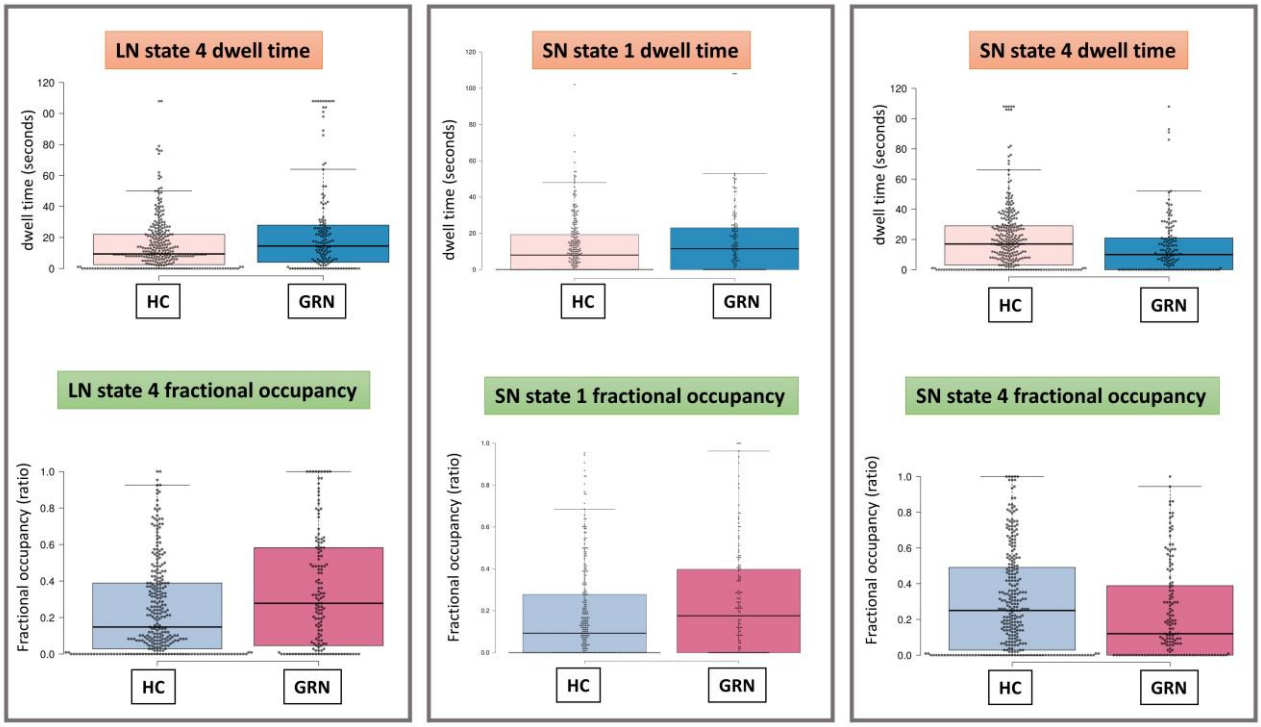

Supplementary Figure 2.

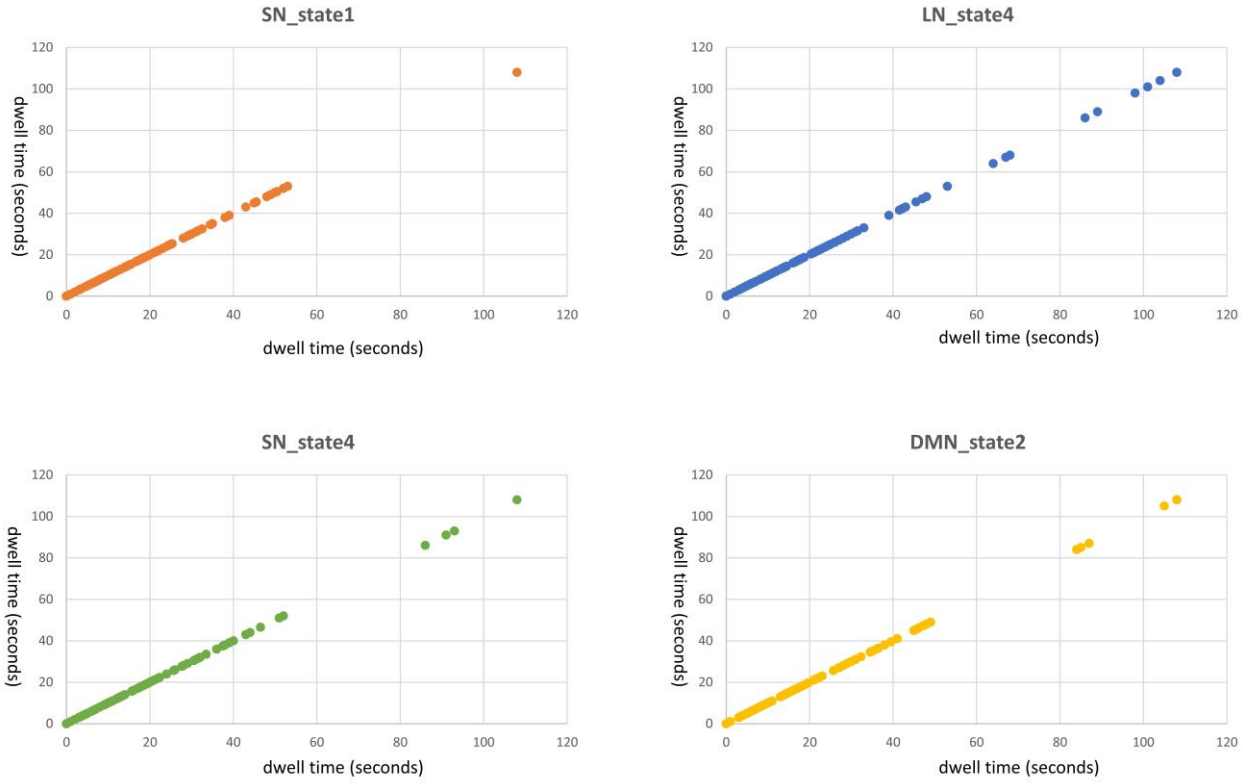

Supplementary Figure 3.